

Label-Only Model Inversion Attacks via Knowledge Transfer

Ngoc-Bao Nguyen^{*1} Keshigeyan Chandrasegaran^{*2‡}

Milad Abdollahzadeh¹ Ngai-Man Cheung^{1†}

¹Singapore University of Technology and Design (SUTD) ²Stanford University

thibaongoc_nguyen@mymail.sutd.edu.sg ngaiman_cheung@sutd.edu.sg

Abstract

In a model inversion (MI) attack, an adversary abuses access to a machine learning (ML) model to infer and reconstruct private training data. Remarkable progress has been made in the white-box and black-box setups, where the adversary has access to the complete model or the model’s soft output respectively. However, there is very limited study in the most challenging but practically important setup: Label-only MI attacks, where the adversary only has access to the model’s predicted label (hard label) without confidence scores nor any other model information.

In this work, we propose LOKT, a novel approach for label-only MI attacks. Our idea is based on transfer of knowledge from the opaque target model to surrogate models. Subsequently, using these surrogate models, our approach can harness advanced white-box attacks. We propose knowledge transfer based on generative modelling, and introduce a new model, Target model-assisted ACGAN (T-ACGAN), for effective knowledge transfer. Our method casts the challenging label-only MI into the more tractable white-box setup. We provide analysis to support that surrogate models based on our approach serve as effective proxies for the target model for MI. Our experiments show that our method significantly **outperforms existing SOTA Label-only MI attack by more than 15% across all MI benchmarks**. Furthermore, our method compares favorably in terms of query budget. Our study highlights rising privacy threats for ML models even when minimal information (i.e., hard labels) is exposed. Our code, demo, models and reconstructed data are available at our project page: <https://ngoc-nguyen-0.github.io/lokt/>

1 Introduction

Model inversion (MI) attacks aim to infer and reconstruct sensitive private samples used in the training of models. MI and their privacy implications have attracted considerable attention recently [1–11]. The model subject to MI is referred to as *target model*. There are three categories of MI attacks: (1) White-box MI, where complete target model information is accessible by the adversary [1–3, 5, 7, 10]; (2) Black-box MI, where target model’s soft labels are accessible [4, 12, 10, 13]; (3) Label-only MI, where only target model’s hard labels are accessible [6]. This paper focuses on label-only MI, which is the most challenging setup as only limited information (hard labels) is available (Fig. 1).

In most existing work, MI attack is formulated as an optimization problem to seek reconstructions that maximize the likelihood under the target model [1–3, 6]. For DNNs, the optimization problems are highly non-linear. When the sensitive private samples are high-dimensional samples (e.g. face

^{*} These authors contributed equally. [‡] Work done while at SUTD.

[†] Corresponding author.

images), the optimizations are ill-posed, even in white-box setups. To overcome such issues, recent MI [1–3, 5, 10, 7, 6, 11] learn distributional priors from public data via GANs [14–17], and solve the optimization problems over GAN latent space rather than the unconstrained image space. For example, MI attacks on face recognition systems could leverage GANs to learn face manifolds from public face images which have no identity intersection with private training images. White-box attacks based on public data and GANs have achieved remarkable success [1–3, 7, 11]. We follow existing work and recent label-only MI [6] and leverage public data in our method. Furthermore, similar to existing work, we use face recognition models as examples of target models.

Research gap. Different from white-box attack, study on label-only attack is limited despite its practical importance, e.g., many practical ML models only expose predicted labels. Focusing on label-only attack and with no knowledge of internal workings of target model nor its confidence score, BREPMI [6] takes a *black-box search* approach to explore the search space iteratively (Fig. 1(a)). To seek reconstructions with high likelihood under target model, [6] proposes to query target model and observe the model’s hard label predictions, and update search directions using *Boundary Repelling* in order to move towards centers of decision regions, where high likelihood reconstructions could be found. However, black-box search in the high-dimensional latent space is extremely challenging.

In this paper, we propose a new approach for Label-Only MI attack using Knowledge Transfer (LOKT). Instead of performing a black-box search approach as demonstrated in [6] and directly searching high-likelihood reconstruction from the opaque target model (Fig. 1(a)), which could be particularly challenging for high-dimensional search space, we propose a different approach. Our approach aims to transfer the decision knowledge of the target model to surrogate models, for which complete model information is accessible. Subsequently, with these surrogate models, we could harness SOTA white box attacks to seek high-likelihood reconstructions (Fig. 1(b)). To obtain the surrogate models, we explore generative modeling [18–22]. In particular, we propose a new Target model-assisted ACGAN, T-ACGAN, which extends ACGAN [23] and leverages our unique problem setup where we have access to the predicted labels of the target model as shown in Fig. 1(d). In particular, by effectively leveraging the target model in discriminator/classifier training, we can explore *synthetic data* for decision knowledge transfer from the target model to the surrogate model. With T-ACGAN capturing the data manifold of public samples, synthetic data is diverse and abundant. We hypothesize that such rich synthetic data could lead to improved decision knowledge transfer. Moreover, as training progresses, T-ACGAN generator learns to improve its conditional generative capabilities, enabling it to produce more balanced synthetic data for surrogate model learning. We explore several surrogate model designs. In one configuration, we employ the discriminator/ classifier of T-ACGAN as the surrogate model. In an alternative design, we utilize the generator of T-ACGAN to train different surrogate model variants. It’s noteworthy that the generator of T-ACGAN can be readily employed for white-box attacks, and its conditional generation capabilities can effectively reduce the search space during inversion. **In addition, we perform analysis to support that our surrogate models are effective proxies for the opaque target model for MI.** (Fig. 1(e)). Overall, our T-ACGAN renders improved surrogate models, resulting in a significant boost in MI attack accuracy (Fig. 1(f)) and reduced number of queries compared to previous SOTA approach. **Our contributions are:**

- We propose LOKT, a new label-only MI by transferring decision knowledge from the target model to surrogate models and performing white-box attacks on the surrogate models (Sec. 4). Our proposed approach is the first to address label-only MI via white-box attacks.
- We propose a new T-ACGAN to leverage generative modeling and the target model for effective knowledge transfer (Sec. 4).
- We perform analysis to support that our surrogate models are effective proxies for the target model for MI (Sec. 5).
- We conduct extensive experiments and ablation to support our claims. Experimental results show that our approach can achieve significant improvement compared to existing SOTA MI attacks (Sec. 6). Additional experiments/ analysis are in Supplementary.

2 Related work

Model Inversion (MI) has particularly alarming consequences in security-sensitive domains, such as face recognition [24–27], medical diagnosis [28–30]. Fredrikson et al. [31] introduces the first

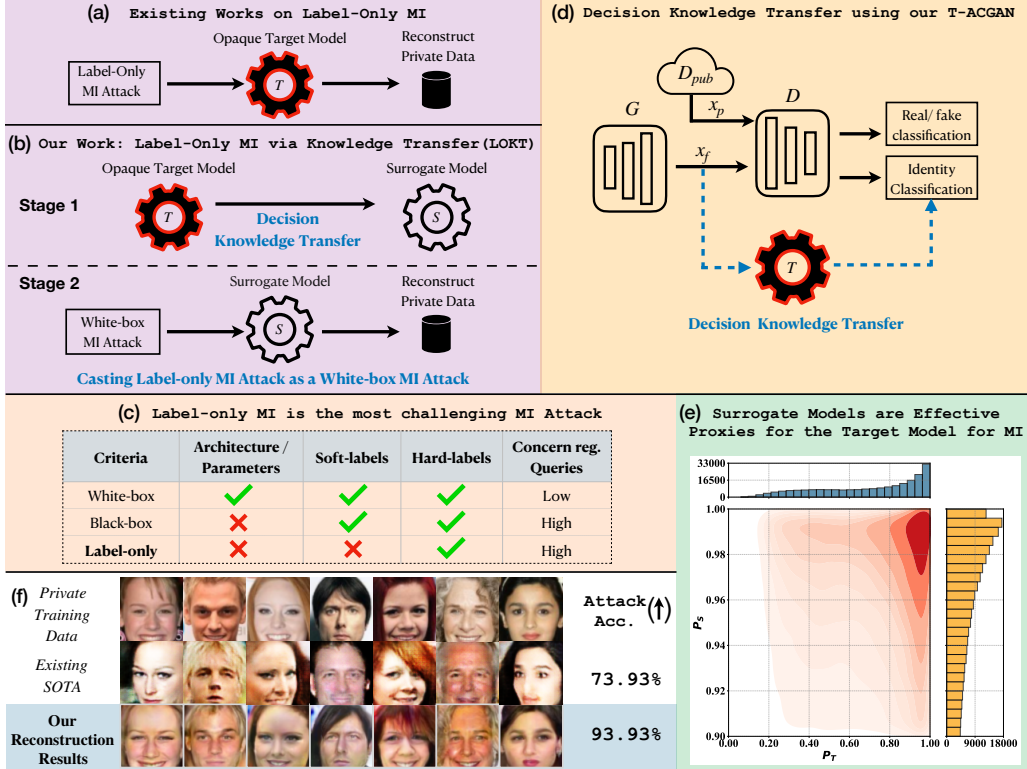


Figure 1: *Overview and our contributions.* (a) Under Label-only model inversion (MI) attack, the Target model T is opaque. (b) **Stage 1:** As our first contribution, we propose a knowledge transfer scheme to render surrogate model(s). (b) **Stage 2:** Then, we cast the Label-only MI attack as a white-box MI attack on surrogate model(s) S . (c) This casting can ease the challenging problem setup of label-only MI attack into a white-box MI attack. To our knowledge, our proposed approach is the first to address label-only MI via white-box MI attacks. (d) We propose T-ACGAN to leverage generative modeling and the target model for effective knowledge transfer to render surrogate model(s). Knowledge transfer renders D (Discriminator) as a surrogate model, and further generated samples of T-ACGAN can be used to train additional surrogate variant S (Sec. 4.3). (e) Our analysis demonstrates that S is an effective proxy for T for MI attack (details in Sec.5). In particular, white-box MI attack on S mimics the white-box attack on opaque T . (f) Our proposed approach significantly improves the Label-only MI attack (e.g. $\approx 20\%$ improvement in standard CelebA benchmark compared to existing SOTA [6]) resulting in significant improvement in private data reconstruction. Best viewed in color.

MI attack for simple linear regression models. Recently, several works extend MI for complex DNNs under different setups. For white-box setup, [1] proposes Generative Model Inversion (GMI) to leverage public data and GAN[32, 33] to constrain the search space. [2] proposes Knowledge-Enriched Distributional Model Inversion (KEDMI) to train an inversion-specific GAN for the attack. [3] proposes Variational Model Inversion (VMI) to apply variational objectives for the attack. Very recent work [7] proposes Pseudo Label-Guided MI (PLG-MI) to apply model’s soft output to train a conditional GAN (cGAN)[34] for white-box attack. LOMMA[11] proposes a better objective function for MI and model augmentation to address MI overfitting. For black-box attack, where model’s soft output is available, [4] proposes to train an inversion model and a decoder to generate target images using predicted scores of the inversion model. [12] proposes an adversarial approach for black-box MI. For label-only attack, [6] proposes BREPMI, the first label-only MI using a black-box Boundary Repelling search. See Supplementary for further discussion of related work.

3 Problem setup

Given a target model T , the goal of MI is to infer private training data \mathcal{D}_{priv} by abusing access to model T . More specifically, given a target class/ identity label y , the adversary aims to reconstruct

an image x which is similar to the images of class y in \mathcal{D}_{priv} . Most MI formulate the inversion as optimization problems to seek the highest likelihood reconstructions for identity y under T . As direct searching for x in the unconstrained image space is ill-posed, many MI attacks [1–3, 7, 6] leverage public dataset \mathcal{D}_{pub} that is the same domain as \mathcal{D}_{priv} , e.g., \mathcal{D}_{priv} and \mathcal{D}_{pub} are facial image datasets. GAN [14] is applied to learn distributional prior from \mathcal{D}_{pub} , and the adversary searches the GAN latent space instead of the unconstrained image space for high-likelihood reconstructions under T :

$$\max_z \log P_T(y|G(z)) \quad (1)$$

Here, G is the generator, and $P_T(y|\cdot)$ is the likelihood of an input for identity y under target model T . White-box attacks apply gradient ascent and some regularization [1–3, 7] to solve Eq. 1, whereas label-only attack BREPMI [6] applies black-box search to tackle Eq. 1. In this paper, we also tackle Eq. 1 under label-only setup, i.e. only the predicted label is available.

4 Approach

Our proposed label-only MI consists of two stages. In stage 1, we learn surrogate models. In stage 2, we apply SOTA white-box attack on the surrogate models. To learn surrogate models, we explore an approach based on GAN and propose a new Target model-assisted ACGAN (T-ACGAN) for effective transfer of decision knowledge. Our T-ACGAN learns the generator G and the discriminator D with classifier head C . In one setup, we directly take $C \circ D$ as the surrogate model*. In another setup, we apply G to generate synthetic data to train another surrogate model S or an ensemble of S . Then, we apply SOTA white-box attack on $C \circ D$, S or the ensemble of S . In our experiments, we show that using $C \circ D$ in a white-box attack can already outperform existing SOTA label-only attack. Using S or an ensemble of S can further improve attack performance. The G obtained from our T-ACGAN can be readily leveraged in the attack stage.

4.1 Baseline

Before discussing our proposed approach, we first discuss a simple baseline for comparison. Given the public data, one could directly use the target model T to label the data and learn the surrogate model S . For $x_p \in \mathcal{D}_{pub}$, we construct (x_p, \tilde{y}) , where $\tilde{y} = T(x_p)$ is pseudo label of *private* identity. We obtain the dataset $\tilde{\mathcal{D}}_{pub}$ with samples (x_p, \tilde{y}) , i.e. $\tilde{\mathcal{D}}_{pub}$ is the public dataset with pseudo labels. We apply $\tilde{\mathcal{D}}_{pub}$ to train S . However, this algorithm suffers from class imbalance. In particular, some private identities could have less resemblance to $x_p \in \mathcal{D}_{pub}$. As a result, for some \tilde{y} , there is only a small number of x_p classified into it, and $\tilde{\mathcal{D}}_{pub}$ is class imbalanced. When using $\tilde{\mathcal{D}}_{pub}$ to train S , minority classes may not gain adequate decision knowledge under T and could perform sub-optimally. In our experiments, we also apply techniques to mitigate the class imbalance in $\tilde{\mathcal{D}}_{pub}$. However, the performance of this baseline approach is inadequate as we will show in the experiments.

4.2 Review of ACGAN

In standard ACGAN [23], we are given a real training dataset with label, i.e., \mathcal{D}_{real} with samples (x_r, y) . The generator G takes a random noise vector z and a class label y as inputs to generate a fake sample x_f . The discriminator D outputs both a probability distribution over sources $P(s|x) = D(x)$, where $s \in \{Real, Fake\}$, and a probability distribution over the class labels, i.e., $P(c|x) = C \circ D(x)$, and c is one of the classes. For real training sample x_r of label y and fake sample $x_f = G(z, y)$ with conditional information y , the loss functions for D , C and G are:

$$\begin{aligned} \mathcal{L}_{D,C} = & -E[\log P(s = Fake|x_f)] - E[\log P(s = Real|x_r)] \\ & - E[\log P(c = y|x_f)] - E[\log P(c = y|x_r)] \end{aligned} \quad (2)$$

$$\mathcal{L}_G = E[\log P(s = Fake|x_f)] - E[\log P(c = y|x_f)] \quad (3)$$

*With a slight abuse of notation we use D to represent the entire discriminator and the discriminator up to and including the penultimate layer in the context of $C \circ D$.

4.3 Our Proposed T-ACGAN and Learning of Surrogate Model

Unlike standard ACGAN setup where we have access to labelled data \mathcal{D}_{real} with samples (x_r, y) , in our setup, we have access to real public data without label: \mathcal{D}_{pub} with samples x_p . *Importantly, we can leverage the target model T to provide pseudo labels for generated samples $x_f = G(z, y)$, which are diverse and abundant.* Our proposed T-ACGAN aims to take advantage of T to provide more diverse and accurate pseudo labelled samples during the training.

D and C Learning. Our T-ACGAN leverages T to assign pseudo labels to the diverse generated samples $x_f = G(z, y)$, i.e., $\tilde{y} = T(x_f)$. We apply samples x_p and (x_f, \tilde{y}) to learn D and C :

$$\begin{aligned} \mathcal{L}_{D,C} = & -E[\log P(s = Fake|x_f)] - E[\log P(s = Real|x_p)] \\ & - E[\log P(c = \tilde{y}|x_f)] \end{aligned} \quad (4)$$

In Eq. 4, the term $E[\log P(c = \tilde{y}|x_f)] = E[\log P(c = \tilde{y}|G(z, y))]$ is different from ACGAN and may look intriguing. Instead of using y as class supervision to train D and C as in ACGAN (Eq. 2), our T-ACGAN takes advantage of T to apply $\tilde{y} = T(G(z, y))$ to train D and C , as \tilde{y} is more accurate conditional information compared with y especially during the initial epochs. *With Eq. 4, our method transfers the decision knowledge of T into D and C via diverse generated samples.* Furthermore, as we can generate diverse pseudo labelled samples (x_f, \tilde{y}) using T and G , pseudo labelled data based on x_p can be omitted. In our experiment, we show that we can achieve good performance using diverse samples (x_f, \tilde{y}) . In T-ACGAN, we utilize public data x_p only for real/fake discrimination.

G Learning. We follow ACGAN training for G , i.e. Eq. 3. With D and C trained with decision knowledge of T in the above step, they provide feedbacks to G to improve its conditional generation in the private label space of T . In our experiment, we analyze y in $x_f = G(z, y)$ and $\tilde{y} = T(x_f)$. As training progresses, G improves its conditional generation, and y and \tilde{y} become more aligned. Note that, as T outputs only hard labels, T cannot be readily applied to provide feedback for G learning.

Surrogate Model. With alternating D and C learning and G learning, we obtain D , C and G . We explore three methods to obtain the surrogate model. • (i) We directly take $C \circ D$ in T-ACGAN as the surrogate model and apply a white-box attack on $C \circ D$. This can be justified as $C \circ D$ is trained based on decision knowledge of T to classify a sample into identities of private training data. • (ii) We apply G of T-ACGAN to generate dataset $\tilde{\mathcal{D}}_{fake}$ with samples (x_f, \tilde{y}) , where $x_f = G(z, y)$ and $\tilde{y} = T(x_f)$. We apply $\tilde{\mathcal{D}}_{fake}$ to train another surrogate model S . • (iii) We use the same dataset $\tilde{\mathcal{D}}_{fake}$ in (ii) to train an ensemble of S of different architectures. As pointed out in [11], using an ensemble of S could improve white-box attack performance.

White-box Attack. With surrogate model $C \circ D$, S or an ensemble of S , any white-box attack can be applied. In our experiments, we show that our surrogate models are effective across a range of white-box attacks (See the Supplementary). Furthermore, G in T-ACGAN can be readily leveraged for performing the attack. Particularly, based on $G(z, y)$ obtained in the above steps, we could reduce the search space during inversion to the latent region corresponding to the target identity y , leading to more efficient search and improved attack accuracy [7].

5 Analysis for justification of surrogate models

In this section, we provide an analysis to justify why our surrogate model could be an effective proxy for T under MI, i.e., *the results of white-box MI attack on our surrogate model be good approximation to that of white-box MI attack on T .* Note that results of white-box MI on T cannot be obtained directly as T exposes only hard labels. To simplify the presentation, we focus our discussion on S . As discussed in Sec. 3, most MI attacks formulate inversion as an optimization problem of seeking reconstructions that achieve highest likelihood under target model. Therefore, when we carry out MI on S with SOTA white-box approaches, we expect to obtain high-likelihood reconstructions under S (or high-likelihood generated samples of GAN under S , see Eq. 1). We use P_S and P_T to denote likelihood of a sample under S and T respectively.

In what follows, we provide analysis to support that S based on our approach would possess an important property of good proxy for T . **Property P1:** *For high-likelihood samples under S , it is likely that they also have high likelihood under T .* See Fig. 1(e) for distribution of generated samples' P_T conditioning on those with high P_S . It can be observed that many have high P_T . Particularly, it is

uncommon for high-likelihood samples under S to have low likelihood under T (see Fig. 1(e) only a few samples have low P_T).

With **Property P1**, the result obtained by white-box on S (which is a high likelihood sample under S) is likely to have a high likelihood under T and could be a good approximation to the result of white-box on T (which is a high likelihood sample under T). In Fig. 1(e), **P1** can be clearly observed[†]. Therefore, S using our approach would possess **P1** and would be a good proxy for T for MI.

Why would S possess property P1? This could be intriguing. After all, T does not expose any likelihood information. The labels of samples assigned by T are the only information available to S during training of S . It does not appear that S can discern low or high-likelihood samples under T .

To discuss why S would possess **P1**, we apply findings and analysis framework of Arpit et al. [35] regarding the general learning dynamics of DNNs. [35] presents a data-centric study of DNN learning with SGD-variants. In [35], “easy samples” are ones that fit better some patterns in the data (and correspondingly “hard samples”). The easy and hard samples exhibit high and low likelihoods in DNNs resp. as discussed in [35]. Furthermore, an important finding from [35] is that, in DNNs learning, the models learn simple and general patterns of the data *first* in the training stage to fit the easy samples.

We apply the framework of [35] to understand our learning of S and the reason why S would possess **P1**. Fig. 2(a) illustrates easy and hard samples in our problem: patterns of face identities can be observed in some samples (easy samples), while other samples (hard samples) exhibit diverse appearance. Similar to [35], Fig. 2(b) shows that these easy and hard face samples tend to have high and low likelihood under T . Fig. 2(c) shows the learning of S on these easy and hard samples at different epochs. Consistent with the “DNNs Learn Patterns First” finding in [35], S learns general identity patterns first to fit the easy samples. Therefore, P_S of easy samples improve at a faster pace in the training, and many of them achieve high P_S . As easy samples tend to have high P_T , we observe **P1** in S . For the hard samples (which tend to have low P_T), it is uncommon for S to achieve high likelihood on them as they do not fit easily to the pattern learned by S .

6 Experiments

In this section, we present extensive experiment results and ablation studies: (i) We show that our proposed T-ACGAN can lead to better surrogate models compared to alternative approaches (Sec. 6.2). (ii) We show that our proposed approach LOKT can significantly outperform the existing SOTA label-only MI attack (Sec. 6.3). (iii) We present additional results (Sec. 6.4) to demonstrate the efficacy of LOKT against SOTA MI defense methods. We further show that LOKT compares favorably in terms of query budget compared to existing SOTA. **Additional experiments/analysis provided in Supplementary.**

6.1 Experimental Setup

To ensure a fair comparison, we adopt the exact experimental setup used in BREPMI [6]. In what follows, we provide details of the experimental setup.

Dataset. We use three datasets, namely CelebA [40], Facescrub [41], and Pubfig83 [42]. We further study Label-Only MI attacks under distribution shift using FFHQ dataset [43] which contains images that vary in terms of background, ethnicity, and age. Following [2, 6], we divide each dataset (CelebA/Facescrub/Pubfig83) into two non-overlapping sets: private set \mathcal{D}_{priv} for training the target model T , and public set \mathcal{D}_{pub} for training GAN/T-ACGAN. More details on datasets and attacked identities can be found in Supplementary.

Target Models. Following [2, 6], we use 3 target models T including VGG16 [38], IR152 [37], and FaceNet64 [36]. All target models are provided in [2, 6].

Table 1: Details of target model T . To showcase the effectiveness of our proposed method, we conduct a comprehensive set of 30 experiments, covering 10 different setups.

\mathcal{D}_{priv}	T	
	Architecture	# classes
CelebA	FaceNet64 [36]	1,000
	IR152 [37]	
	VGG16 [38]	
	BiDO-HSIC [39]	
	MID [9]	
Facescrub	FaceNet64 [36]	200
Pubfig83	FaceNet64	50

[†]Fig. 1(e) are P_T and P_S of $x_f = G(z, y)$ from our T-ACGAN. More details in Supp.

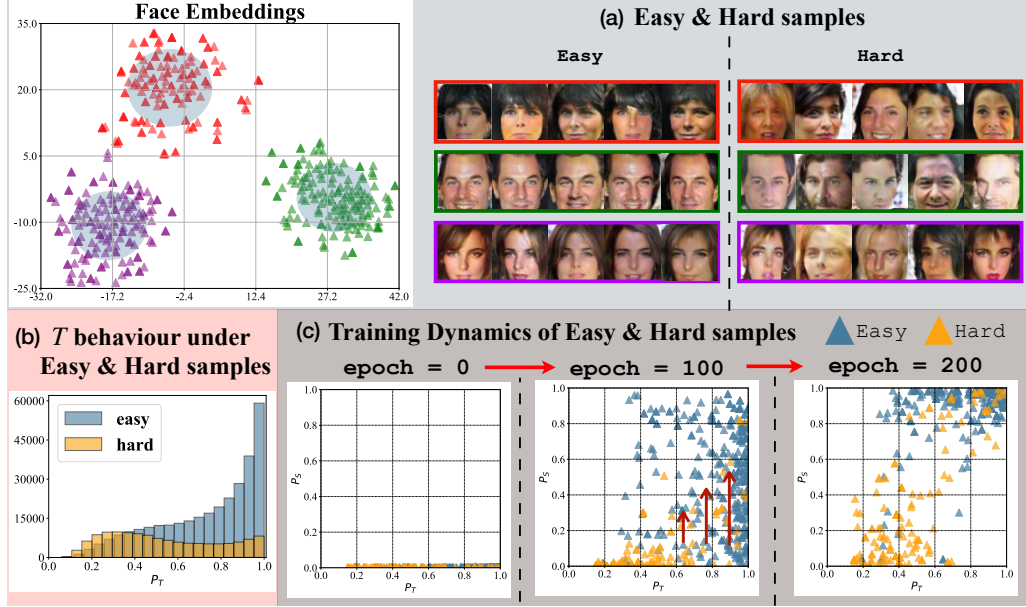


Figure 2: We apply the framework of [35] to analyze learning dynamics of S to reason why S possesses property **P1**, and therefore could be an effective proxy for T under MI. We analyze generated samples x_f from our T-ACGAN for 3 identities (IDs 20, 16, 36). Note that x_f analysis is relevant as generated samples are used in MI attacks. (a): We analyze face embeddings of x_f extracted from publicly available SOTA face recognition model here. Different clusters and different distances from cluster centroids can be observed, suggesting patterns of face identities in some samples (easy samples) while diverse appearance in other samples (hard samples). We use distances from centroids to identify easy samples x_f^e and hard samples x_f^h (easy samples are indicated using transparent blue circle for each ID in the visualization). Visualization of x_f^e and x_f^h in image space further demonstrates identity patterns in x_f^e and diverse appearance in x_f^h . (b): Similar to [35], we observe that x_f^e and x_f^h tend to have high and low likelihood under T (P_T) resp (training data). (c): We track likelihood under S (P_S) for x_f^e and x_f^h during the training of S . As training progresses, P_S of x_f^e and x_f^h improve, and samples move up vertically (note that P_T of samples do not change). Consistent with the “DNNs Learn Patterns First” finding in [35], S learns general identity patterns first to fit the easy samples. Therefore, P_S of x_f^e improve at a faster pace in the training, and many of them achieve high P_S at epoch = 200. As x_f^e tend to have high P_T , we observe property **P1** in S . For x_f^h (many of them tend to have low P_T), it is uncommon for S to achieve high likelihood on them as they do not fit easily to the pattern learned by S . **See Supplementary for additional details and analysis.** Best viewed in color.

Additionally, we use the following methods/ models for evaluating the attack performance under SOTA MI defense methods: • BiDO-HSIC [39][‡]. • MID [9][§]. The details are included in Table 1.

Evaluation Metrics. Following [6, 11, 2], we use the following metrics to quantitatively evaluate the performance of MI attacks. Further, we also conduct user studies to assess the quality of reconstructed data (Sec. 6.5).

- **Attack Accuracy (Attack acc.):** Following [1, 2, 6], we utilize an evaluation model, E , which employs a distinct architecture and is trained on \mathcal{D}_{priv} [¶]. E serves as a proxy for human inspection [1]. Higher attack accuracy indicates superior performance.
- **KNN Distance (KNN dt.):** The KNN distance indicates the shortest distance between the reconstructed image of a specific identity and its private images. Specifically, the shortest distance is computed using the l_2 distance in the feature space, using the evaluation model’s penultimate layer.

[‡]https://github.com/AlanPeng0897/Defend_MI

[§]<https://github.com/Jiachen-T-Wang/mi-defense>

[¶]Following previous work, E can also be trained on \mathcal{D}_{priv} and samples from additional identities. This could improve generalization of E for accurate evaluation.

A smaller KNN distance signifies that the reconstructed images are more closely aligned with the private images of the target identity.

6.2 Training surrogate model with different algorithms

In this section, we demonstrate that our proposed T-ACGAN can lead to better surrogate models for MI. We describe a set of alternative approaches that can be used to train surrogate models using \mathcal{D}_{pub} and compare the performance of these approaches with our proposed method. Specifically, we consider a set of five algorithms, which can be broadly classified into three categories, for learning the surrogate model S :

- **Directly use the public dataset \mathcal{D}_{pub} .** We present two methods to train S : • **Direct I.** We train S using the public dataset labelled with target model, *i.e.* $\tilde{\mathcal{D}}_{pub}$ with samples (x_p, \tilde{y}) , $x_p \in \mathcal{D}_{pub}$, $\tilde{y} = T(x_p)$; see Sec. 4.1. • **Direct II.** We apply data augmentation to $\tilde{\mathcal{D}}_{pub}$ of Direct I to reduce the class imbalance in Direct I, followed by training S using the newly more balanced dataset.
- **Training an ACGAN.** We provide two versions: • **ACGAN I.** We train an ACGAN model on $\tilde{\mathcal{D}}_{pub}$ used in Direct I. • **ACGAN II.** We train an ACGAN model on augmented $\tilde{\mathcal{D}}_{pub}$ used in Direct II. As $C \circ D$ in ACGAN serves as a classifier, we use $C \circ D$ for MI attacks.
- **Training proposed T-ACGAN.** We use our proposed method described in Section 4.3 to train T-ACGAN. Similar to ACGAN I and II, we use $C \circ D$ after training T-ACGAN for the attack.

For this comparison, we utilize the following settings: T = FaceNet64, \mathcal{D}_{priv} = CelebA, \mathcal{D}_{pub} = CelebA. Both ACGAN and T-ACGAN adopt the SNResnet architecture [34, 44]. To ensure a fair comparison, we use the same architecture as $C \circ D$ in ACGAN and T-ACGAN for the surrogate model S in Direct I and Direct II. Detailed architecture specifications can be found in the Supplementary. After training the models, we employ the widely-used KEDMI [2] as the white-box attack on the trained surrogate models. Table 2 presents the results. The effectiveness of T-ACGAN in training surrogate models for MI attacks can be observed.

Table 2: We compare different approaches to train surrogate model for MI attacks. We utilize the following settings: T = FaceNet64, \mathcal{D}_{priv} = CelebA, \mathcal{D}_{pub} = CelebA, and employ the KEDMI[2] for MI attacks.

Algorithm	Attack acc. \uparrow	KNN dt. \downarrow
Direct I	5.87 \pm 1.65	1936.12
Direct II	9.60 \pm 2.22	1890.16
ACGAN I	6.47 \pm 2.15	1771.26
ACGAN II	7.87 \pm 3.10	1785.20
T-ACGAN	42.07 \pm 3.46	1473.99

6.3 Comparison against SOTA label-only MI attack

Standard MI attack setup. In this section, we present the results obtained from the standard attack setup on three datasets: CelebA, Facescrub, and Pubfig83, as detailed in Table 3. We evaluate three designs of surrogate: • (i) We directly use $C \circ D$ from our T-ACGAN as the surrogate model. The architecture of T-ACGAN can be found in the supplementary material. • (ii) We utilize the synthetic data generated by G of our T-ACGAN and label it using the target classifier T to train another surrogate model, denoted as $S = \text{Densenet-161}$ [45]. • (iii) We employ the same data as in (ii) to train an ensemble of surrogate models, denoted as S_{en} , using different architectures including Densenet-121, Densenet-161, and Densenet-169.

We compare our results with the state-of-the-art (SOTA) label-only MI attack BREPMI [6]. To conduct our attacks, we utilize white-box PLGMI [7] on the surrogate models. Since PLGMI performs attacks using a conditional GAN trained with white-box access of the target classifier, we replace it with our T-ACGAN, which becomes available for use after training the surrogate models.

Our proposed method LOKT demonstrates a significant improvement in Attack accuracy and KNN distance compared to the SOTA label-only MI attack BREPMI [6]. Our top 1 attack accuracies are better than BREPMI from 17.2% to 29.87% across all setups when we utilize the ensemble S_{en} .

Fig. 1 (f) presents a visual comparison of various methods under the setup \mathcal{D}_{priv} = CelebA, \mathcal{D}_{pub} = CelebA. **More results are available in the Supplementary.** Results clearly indicate that LOKT produces images that are closer to the ground truth (private data) compared to BREPMI [6]. This outcome provides strong evidence of the effectiveness of our approach in generating realistic images that closely resemble private data, which is critical for conducting successful MI attacks.

MI attacks under large distribution shift. Table 3 compares the MI attack results in the large distribution shift setup, where we use \mathcal{D}_{pub} = FFHQ, \mathcal{D}_{priv} = CelebA/ Facescrub/ Pubfig83, and

Table 3: We conduct comprehensive experiments to compare our proposed method LOKT and existing SOTA BREPMI [6] across standard MI attack benchmarks. Specifically, we evaluate the performance of our three proposed designs of surrogate, namely $C \circ D$, S , and S_{en} , while BREPMI performs black-box search on T directly. We highlight the best results in each setup in **bold**.

Setup	Attack	Attack acc. \uparrow	KNN dt. \downarrow	Setup	Attack	Attack acc. \uparrow	KNN dt. \downarrow
T = FaceNet64	BREPMI	73.93 \pm 4.98	1284.41	T = FaceNet64	BREPMI	55.60 \pm 4.34	1012.83
\mathcal{D}_{priv} = CelebA	$C \circ D$	81.00 \pm 4.79	1298.63	\mathcal{D}_{priv} = Pubfig83	$C \circ D$	74.80 \pm 5.93	924.58
\mathcal{D}_{pub} = CelebA	LOKT S	92.80 \pm 2.59	1207.25	\mathcal{D}_{pub} = Pubfig83	LOKT S	61.60 \pm 3.58	993.44
	S_{en}	93.93 \pm 2.78	1181.72		S_{en}	80.00 \pm 3.16	883.52
T = IR152	BREPMI	71.47 \pm 5.32	1277.23	T = FaceNet64	BREPMI	72.80 \pm 3.90	971.51
\mathcal{D}_{priv} = CelebA	$C \circ D$	72.07 \pm 4.03	1358.94	\mathcal{D}_{priv} = Pubfig83	$C \circ D$	85.60 \pm 2.61	914.15
\mathcal{D}_{pub} = CelebA	LOKT S	89.80 \pm 2.33	1220.00	\mathcal{D}_{pub} = FFHQ	LOKT S	88.40 \pm 2.97	920.99
	S_{en}	92.13 \pm 2.06	1206.78		S_{en}	94.40 \pm 3.85	862.24
T = VGG16	BREPMI	57.40 \pm 4.92	1376.94	T = FaceNet64	BREPMI	40.20 \pm 6.60	1236.4
\mathcal{D}_{priv} = CelebA	$C \circ D$	71.33 \pm 4.39	1364.47	\mathcal{D}_{priv} = Facescrub	$C \circ D$	45.70 \pm 4.00	1296.29
\mathcal{D}_{pub} = CelebA	LOKT S	85.60 \pm 3.03	1252.09	\mathcal{D}_{pub} = Facescrub	LOKT S	53.20 \pm 5.29	1280.70
	S_{en}	87.27 \pm 1.97	1246.71		S_{en}	58.60 \pm 4.86	1225.13
T = FaceNet64	BREPMI	43.00 \pm 5.14	1470.55	T = FaceNet64	BREPMI	37.30 \pm 3.99	1456.59
\mathcal{D}_{priv} = CelebA	$C \circ D$	43.27 \pm 3.53	1516.18	\mathcal{D}_{priv} = Facescrub	$C \circ D$	44.50 \pm 5.98	1403.73
\mathcal{D}_{pub} = FFHQ	LOKT S	59.13 \pm 2.77	1437.86	\mathcal{D}_{pub} = FFHQ	LOKT S	47.20 \pm 4.39	1404.85
	S_{en}	62.07 \pm 3.89	1428.04		S_{en}	53.70 \pm 4.57	1338.67

Table 4: We report Label-only MI Attack results under SOTA defense models namely BiDO [39] and MID [9]. We use \mathcal{D}_{priv} = CelebA, \mathcal{D}_{pub} = CelebA. We highlight the best results in **bold**.

Setup	Attack	Attack acc. \uparrow	KNN dt. \downarrow
T = BiDO [39]	BREPMI[6]	37.40 \pm 3.66	1500.45
\mathcal{D}_{priv} = CelebA	$C \circ D$	45.73 \pm 5.94	1493.48
\mathcal{D}_{pub} = CelebA	LOKT S	58.53 \pm 4.87	1427.22
	S_{en}	60.73 \pm 3.07	1395.93
T = MID [9]	BREPMI[6]	39.20 \pm 4.19	1458.61
\mathcal{D}_{priv} = CelebA	$C \circ D$	44.13 \pm 3.54	1475.73
\mathcal{D}_{pub} = CelebA	LOKT S	55.33 \pm 4.40	1393.76
	S_{en}	60.33 \pm 4.76	1374.34

Table 5: The comparison of the number of queries (in millions) used by LOKT and BREPMI [6]. The attacks using S and S_{en} consume additional 500k queries comparing to $C \circ D$ to label the synthetic images to train S and S_{en} . Our results show that we use fewer number of queries than BREPMI in all setups.

T	LOKT $C \circ D$	LOKT S/S_{en}	BREPMI
FaceNet64	12.16	12.66	17.98
IR152	12.16	12.66	18.06
VGG16	12.16	12.66	18.12
BiDO-HSIC	12.16	12.66	18.39
MID	12.16	12.66	18.25

T = FaceNet64. The attack results of BREPMI drop significantly (by 30.93% for CelebA and 2.9% for Facescrub), while the results for Pubfig83 notably increase, which can be attributed to the small size of the Pubfig83 dataset [6]. Our proposed method outperforms BREPMI, with the top 1 attack accuracies increase from 16.40% to 21.60% for all setups. Moreover, the KNN distance indicates that our reconstructed images are closer to the private data than those reconstructed by BREPMI.

6.4 Additional results

MI attack results using MI defense model. We investigate the attacks on the MI defense model (see Table 4). Specifically, we utilize the SOTA defense model BiDO-HSIC [39] and MID [9]. Our results indicate that BiDO-HSIC successfully reduce the effectiveness of the white-box SOTA attack, PLGMI, by 9.57% (See the result in the Supplementary). In the label-only setup, the performance of BREPMI becomes relatively low with attack accuracy of only 37.40% for BiDO-HSIC [39] and 39.20% for MID [9]. In contrast, our approach achieves a much higher attack accuracy of 60.73% and 60.33%, almost doubling the performance of BREPMI. These results demonstrate that our approach is effective in conducting MI attacks on MI defense models, even in scenarios where the adversary has limited information about the target classifier.

High resolution. We conduct the experiment with high resolution images which has not been addressed yet for label-only setup [6]. In particular, we train a new target classifier T = Resnet-152 using CelebA setup with the image size = 128×128 . For fair comparison between BREPMI and our proposed method, T-ACGAN has the same GAN architectures used by BREPMI. The details of the architecture can be found in the Supplementary.

The results are shown in Table 6. LOKT outperforms BREPMI, with top 1 accuracy surpassing BREPMI by 20.27%. Our inverted images are closer to private training samples than BREPMI

Table 6: We conduct the experiment with higher resolution images. We use $T = \text{Resnet-152}$, $\mathcal{D}_{priv} = \text{CelebA}$, $\mathcal{D}_{pub} = \text{CelebA}$, image size = 128×128 . The natural accuracy of T is 86.07%. We highlight the best results in **bold**.

Setup	Attack	Attack acc. \uparrow	KNN dt. \downarrow
$T = \text{IR152}$	BREPMI[6]	50.33 ± 4.71	1389.09
$\mathcal{D}_{priv} = \text{CelebA}$	$C \circ D$	66.87 ± 3.93	1356.53
$\mathcal{D}_{pub} = \text{CelebA}$	LOKT S	66.80 ± 3.83	1341.04
	S_{en}	70.60 ± 4.43	1320.16

Table 7: User study results. Our human study reveals that users distinctly favor our approach, with 64.30% user preference for images reconstructed using our proposed approach, LOKT, compared to BREPMI’s lower 35.70% user preference.

Method	User Preference (\uparrow)
BREPMI	35.70%
LOKT	64.30%

(smaller KNN distance). We believe our study can provide new insight on the effectiveness of SOTA label-only attack at a higher resolution of 128×128 , paving the way to future label-only model inversion attacks at resolutions beyond 128×128 .

Query budget. In this experiment, we compare query budget between our proposed method and BREPMI [2]. In the BREPMI, queries to the target classifier T are required to identify the initial points for attacking and estimate the gradients during the attack. In our method, queries to T are required to label the synthetic data during the training of T-ACGAN to obtain $C \circ D$, and additional 500k queries to label generated images of T-ACGAN to train S and the ensemble S_{en} . For comparison, as shown in Table 5, we use $\mathcal{D}_{priv} = \text{CelebA}$ and $\mathcal{D}_{pub} = \text{CelebA}$. The results show that our proposed method requires 30% fewer queries compared to BREPMI.

6.5 User study

User study setup. In this section, we go beyond objective metrics and consider subjective evaluation of MI attacks. In particular, we conduct a human study to understand the efficacy of our proposed method, LOKT, compared to BREPMI. We follow the setup by [10] for human study and use Amazon Mechanical Turk (MTurk) for experiments. The user interface is provided in the Supplementary. In this study, users are shown 5 real images of a person (identity) as reference. Then users are required to compare the 5 real images with two inverted images: one from our method (LOKT), the other from BREPMI. We use $\mathcal{D}_{priv} = \text{CelebA}$, $\mathcal{D}_{pub} = \text{CelebA}$ and $T = \text{FaceNet64}$. Following [10], we randomly selected 50 identities with 10 unique users evaluating each task accounting to 1000 comparison pairs.

User study results. We report the user study results in Table 7. Our human study reveals that users distinctly favor our approach, with 64.30% user preference for images reconstructed using our proposed approach, in contrast to BREPMI’s lower 35.70% user preference. These subjective evaluations further show the efficacy of our proposed method, LOKT, in the challenging label-only MI setup.

7 Discussion

Conclusion. Instead of performing a black-box search approach as in existing SOTA, we propose a new label-only MI approach (LOKT) by transferring decision knowledge from the target model to surrogate models and performing white-box attacks on the surrogate models. To obtain the surrogate models, we propose a new T-ACGAN to leverage generative modeling and the target model for effective knowledge transfer. Using findings of general learning dynamics of DNNs, we conduct analysis to support that our surrogate models are effective proxies for the target model under MI. We perform extensive experiments and ablation to support our claims and demonstrate significant improvement over existing SOTA.

Broader Impacts. Understanding model inversion attacks holds significance as AI models continue to see widespread deployment across various applications. By studying and understanding the approaches and methodologies for model inversion, researchers can develop good practices in deploying AI models and robust defense mechanisms for different applications esp. those involving sensitive training data. It is important to emphasize that the objective of model inversion research is to raise awareness of potential privacy threats and bolster our collective defenses.

Limitations. While our experiments are extensive compared to previous works, practical applications involve different types of private training datasets such as healthcare data. Nevertheless, our assumptions are general, and we believe our findings can be applied to a broader range of applications.

Acknowledgements. This research is supported by the National Research Foundation, Singapore under its AI Singapore Programmes (AISG Award No.: AISG2-TC-2022-007) and SUTD project PIE-SGP-AI-2018-01. This research work is also supported by the Agency for Science, Technology and Research (A*STAR) under its MTC Programmatic Funds (Grant No. M23L7b0021). This material is based on the research/work support in part by the Changi General Hospital and Singapore University of Technology and Design, under the HealthTech Innovation Fund (HTIF Award No. CGH-SUTD-2021-004). We thank anonymous reviewers for their insightful feedback.

References

- [1] Yuheng Zhang, Ruoxi Jia, Hengzhi Pei, Wenxiao Wang, Bo Li, and Dawn Song. The secret revealer: Generative model-inversion attacks against deep neural networks. In *Proceedings of the IEEE/CVF Conference on Computer Vision and Pattern Recognition*, pages 253–261, 2020.
- [2] Si Chen, Mostafa Kahla, Ruoxi Jia, and Guo-Jun Qi. Knowledge-enriched distributional model inversion attacks. In *Proceedings of the IEEE/CVF international conference on computer vision*, pages 16178–16187, 2021.
- [3] Kuan-Chieh Wang, Yan Fu, Ke Li, Ashish Khisti, Richard Zemel, and Alireza Makhzani. Variational model inversion attacks. *Advances in Neural Information Processing Systems*, 34:9706–9719, 2021.
- [4] Ziqi Yang, Jiye Zhang, Ee-Chien Chang, and Zhenkai Liang. Neural network inversion in adversarial setting via background knowledge alignment. In *Proceedings of the 2019 ACM SIGSAC Conference on Computer and Communications Security*, pages 225–240, 2019.
- [5] Lukas Struppek, Dominik Hintersdorf, Antonio De Almeida Correia, Antonia Adler, and Kristian Kersting. Plug and play attacks: Towards robust and flexible model inversion attacks. In Kamalika Chaudhuri, Stefanie Jegelka, Le Song, Csaba Szepesvari, Gang Niu, and Sivan Sabato, editors, *Proceedings of the 39th International Conference on Machine Learning*, volume 162 of *Proceedings of Machine Learning Research*, pages 20522–20545. PMLR, 17–23 Jul 2022.
- [6] Mostafa Kahla, Si Chen, Hoang Anh Just, and Ruoxi Jia. Label-only model inversion attacks via boundary repulsion. In *Proceedings of the IEEE/CVF Conference on Computer Vision and Pattern Recognition*, pages 15045–15053, 2022.
- [7] Xiaojian Yuan, Kejiang Chen, Jie Zhang, Weiming Zhang, Nenghai Yu, and Yang Zhang. Pseudo label-guided model inversion attack via conditional generative adversarial network. *Thirty Seventh AAAI Conference on Artificial Intelligence (AAAI 23)*, 2023.
- [8] Mahdi Khosravy, Kazuaki Nakamura, Yuki Hirose, Naoko Nitta, and Noboru Babaguchi. Model inversion attack by integration of deep generative models: Privacy-sensitive face generation from a face recognition system. *IEEE Transactions on Information Forensics and Security*, 17:357–372, 2022.
- [9] Tianhao Wang, Yuheng Zhang, and Ruoxi Jia. Improving robustness to model inversion attacks via mutual information regularization. In *Proceedings of the AAAI Conference on Artificial Intelligence*, volume 35, pages 11666–11673, 2021.
- [10] Shengwei An, Guan hong Tao, Qiuling Xu, Yingqi Liu, Guangyu Shen, Yuan Yao, Jingwei Xu, and Xiangyu Zhang. Mirror: Model inversion for deep learning network with high fidelity. In *Proceedings of the 29th Network and Distributed System Security Symposium*, 2022.
- [11] Ngoc-Bao Nguyen, Keshigeyan Chandrasegaran, Milad Abdollahzadeh, and Ngai-Man Cheung. Rethinking model inversion attacks against deep neural networks. In *Proceedings of the IEEE/CVF Conference on Computer Vision and Pattern Recognition (CVPR)*, pages 16384–16393, June 2023.
- [12] Ulrich Aivodji, Sebastien Gambs, and Timon Ther. Gamin: An adversarial approach to black-box model inversion. In *The AAAI Workshop on Privacy-Preserving Artificial Intelligence*, 2020.
- [13] Gyojin Han, Jaehyun Choi, Haeil Lee, and Junmo Kim. Reinforcement learning-based black-box model inversion attacks. In *Proceedings of the IEEE/CVF Conference on Computer Vision and Pattern Recognition (CVPR)*, pages 20504–20513, June 2023.
- [14] Ian Goodfellow, Jean Pouget-Abadie, Mehdi Mirza, Bing Xu, David Warde-Farley, Sherjil Ozair, Aaron Courville, and Yoshua Bengio. Generative adversarial nets. In *Advances in Neural Information Processing Systems*, 2014.

- [15] Tero Karras, Samuli Laine, and Timo Aila. A style-based generator architecture for generative adversarial networks. In *Proceedings of the IEEE/CVF Conference on Computer Vision and Pattern Recognition (CVPR)*, June 2019.
- [16] Tero Karras, Samuli Laine, Miika Aittala, Janne Hellsten, Jaakko Lehtinen, and Timo Aila. Analyzing and improving the image quality of stylegan. In *IEEE/CVF Conference on Computer Vision and Pattern Recognition (CVPR)*, June 2020.
- [17] Keshigeyan Chandrasegaran, Ngoc-Trung Tran, and Ngai-Man Cheung. A closer look at fourier spectrum discrepancies for cnn-generated images detection. In *Proceedings of the IEEE/CVF conference on computer vision and pattern recognition*, pages 7200–7209, 2021.
- [18] Milad Abdollahzadeh, Toubia Malekzadeh, Christopher TH Teo, Keshigeyan Chandrasegaran, Guimeng Liu, and Ngai-Man Cheung. A survey on generative modeling with limited data, few shots, and zero shot. *arXiv preprint arXiv:2307.14397*, 2023.
- [19] Yunqing Zhao, Chao Du, Milad Abdollahzadeh, Tianyu Pang, Min Lin, Shuicheng Yan, and Ngai-Man Cheung. Exploring incompatible knowledge transfer in few-shot image generation. In *Proceedings of the IEEE/CVF Conference on Computer Vision and Pattern Recognition*, pages 7380–7391, 2023.
- [20] Christopher TH Teo, Milad Abdollahzadeh, and Ngai-Man Cheung. Fair generative models via transfer learning. In *Proceedings of the AAAI Conference on Artificial Intelligence*, volume 37, pages 2429–2437, 2023.
- [21] Yunqing Zhao, Keshigeyan Chandrasegaran, Milad Abdollahzadeh, and Ngai-Man Man Cheung. Few-shot image generation via adaptation-aware kernel modulation. *Advances in Neural Information Processing Systems*, 35:19427–19440, 2022.
- [22] Christopher TH Teo, Milad Abdollahzadeh, and Ngai-Man Cheung. On measuring fairness in generative models. *Advances in Neural Information Processing Systems*, 36, 2023.
- [23] Augustus Odena, Christopher Olah, and Jonathon Shlens. Conditional image synthesis with auxiliary classifier gans. In *International conference on machine learning*, pages 2642–2651. PMLR, 2017.
- [24] Florian Schroff, Dmitry Kalenichenko, and James Philbin. Facenet: A unified embedding for face recognition and clustering. In *Proceedings of the IEEE conference on computer vision and pattern recognition*, pages 815–823, 2015.
- [25] Yaniv Taigman, Ming Yang, Marc’ Aurelio Ranzato, and Lior Wolf. Deepface: Closing the gap to human-level performance in face verification. In *Proceedings of the IEEE conference on computer vision and pattern recognition*, pages 1701–1708, 2014.
- [26] Qiang Meng, Shichao Zhao, Zhida Huang, and Feng Zhou. Magface: A universal representation for face recognition and quality assessment. In *Proceedings of the IEEE/CVF Conference on Computer Vision and Pattern Recognition*, pages 14225–14234, 2021.
- [27] Yuge Huang, Yuhan Wang, Ying Tai, Xiaoming Liu, Pengcheng Shen, Shaoxin Li, Jilin Li, and Feiyue Huang. Curricularface: adaptive curriculum learning loss for deep face recognition. In *proceedings of the IEEE/CVF conference on computer vision and pattern recognition*, pages 5901–5910, 2020.
- [28] Benoit Dufumier, Pietro Gori, Julie Victor, Antoine Grigis, Michele Wessa, Paolo Brambilla, Pauline Favre, Mircea Polosan, Colm Mcdonald, Camille Marie Piguat, et al. Contrastive learning with continuous proxy meta-data for 3d mri classification. In *Medical Image Computing and Computer Assisted Intervention—MICCAI 2021: 24th International Conference, Strasbourg, France, September 27–October 1, 2021, Proceedings, Part II* 24, pages 58–68. Springer, 2021.
- [29] Jiawei Yang, Hanbo Chen, Jiangpeng Yan, Xiaoyu Chen, and Jianhua Yao. Towards better understanding and better generalization of few-shot classification in histology images with contrastive learning. *International Conference on Learning Representations*, 2022.
- [30] Jonas Dippel, Steffen Vogler, and Johannes Höhne. Towards fine-grained visual representations by combining contrastive learning with image reconstruction and attention-weighted pooling. *arXiv preprint arXiv:2104.04323*, 2021.
- [31] Matthew Fredrikson, Eric Lantz, Somesh Jha, Simon Lin, David Page, and Thomas Ristenpart. Privacy in pharmacogenetics: An {End-to-End} case study of personalized warfarin dosing. In *23rd USENIX Security Symposium (USENIX Security 14)*, pages 17–32, 2014.

- [32] Ian Goodfellow, Jean Pouget-Abadie, Mehdi Mirza, Bing Xu, David Warde-Farley, Sherjil Ozair, Aaron Courville, and Yoshua Bengio. Generative adversarial networks. *Communications of the ACM*, 63(11):139–144, 2020.
- [33] Martin Arjovsky, Soumith Chintala, and Léon Bottou. Wasserstein generative adversarial networks. In *International conference on machine learning*, pages 214–223. PMLR, 2017.
- [34] Takeru Miyato and Masanori Koyama. cGANs with projection discriminator. In *International Conference on Learning Representations*, 2018.
- [35] Devansh Arpit, Stanislaw Jastrzebski, Nicolas Ballas, David Krueger, Emmanuel Bengio, Maxinder S. Kanwal, Tegan Maharaj, Asja Fischer, Aaron Courville, Yoshua Bengio, and Simon Lacoste-Julien. A closer look at memorization in deep networks. In *ICML*, 2017.
- [36] Yu Cheng, Jian Zhao, Zhecan Wang, Yan Xu, Karlekar Jayashree, Shengmei Shen, and Jiashi Feng. Know you at one glance: A compact vector representation for low-shot learning. In *Proceedings of the IEEE International Conference on Computer Vision Workshops*, pages 1924–1932, 2017.
- [37] Kaiming He, Xiangyu Zhang, Shaoqing Ren, and Jian Sun. Deep residual learning for image recognition. In *Proceedings of the IEEE conference on computer vision and pattern recognition*, pages 770–778, 2016.
- [38] Karen Simonyan and Andrew Zisserman. Very deep convolutional networks for large-scale image recognition. *arXiv preprint arXiv:1409.1556*, 2014.
- [39] Xiong Peng, Feng Liu, Jingfeng Zhang, Long Lan, Junjie Ye, Tongliang Liu, and Bo Han. Bilateral dependency optimization: Defending against model-inversion attacks. In *KDD*, 2022.
- [40] Ziwei Liu, Ping Luo, Xiaogang Wang, and Xiaoou Tang. Deep learning face attributes in the wild. In *Proceedings of the IEEE international conference on computer vision*, pages 3730–3738, 2015.
- [41] Hong-Wei Ng and Stefan Winkler. A data-driven approach to cleaning large face datasets. In *2014 IEEE international conference on image processing (ICIP)*, pages 343–347. IEEE, 2014.
- [42] Nicolas Pinto, Zak Stone, Todd Zickler, and David Cox. Scaling up biologically-inspired computer vision: A case study in unconstrained face recognition on facebook. In *CVPR 2011 WORKSHOPS*, pages 35–42. IEEE, 2011.
- [43] Tero Karras, Samuli Laine, and Timo Aila. A style-based generator architecture for generative adversarial networks. In *Proceedings of the IEEE/CVF conference on computer vision and pattern recognition*, pages 4401–4410, 2019.
- [44] Takeru Miyato, Toshiki Kataoka, Masanori Koyama, and Yuichi Yoshida. Spectral normalization for generative adversarial networks. In *International Conference on Learning Representations*, 2018.
- [45] Gao Huang, Zhuang Liu, Laurens Van Der Maaten, and Kilian Q Weinberger. Densely connected convolutional networks. In *Proceedings of the IEEE conference on computer vision and pattern recognition*, pages 4700–4708, 2017.
- [46] Sunandini Sanyal, Sravanti Addepalli, and R Venkatesh Babu. Towards data-free model stealing in a hard label setting. In *Proceedings of the IEEE/CVF Conference on Computer Vision and Pattern Recognition*, pages 15284–15293, 2022.
- [47] Mark Sandler, Andrew Howard, Menglong Zhu, Andrey Zhmoginov, and Liang-Chieh Chen. Mobilenetv2: Inverted residuals and linear bottlenecks. In *Proceedings of the IEEE conference on computer vision and pattern recognition*, pages 4510–4520, 2018.
- [48] Brett Koonce and Brett Koonce. Mobilenetv3. *Convolutional Neural Networks with Swift for Tensorflow: Image Recognition and Dataset Categorization*, pages 125–144, 2021.
- [49] Mingxing Tan and Quoc Le. Efficientnet: Rethinking model scaling for convolutional neural networks. In *International conference on machine learning*, pages 6105–6114. PMLR, 2019.
- [50] Ilya Loshchilov and Frank Hutter. SGDR: stochastic gradient descent with warm restarts. In *5th International Conference on Learning Representations, ICLR 2017, Toulon, France, April 24–26, 2017, Conference Track Proceedings*. OpenReview.net, 2017.
- [51] Matt Fredrikson, Somesh Jha, and Thomas Ristenpart. Model inversion attacks that exploit confidence information and basic countermeasures. In *Proceedings of the 22nd ACM SIGSAC conference on computer and communications security*, pages 1322–1333, 2015.

- [52] Keshigeyan Chandrasegaran, Ngoc-Trung Tran, Yunqing Zhao, and Ngai-Man Cheung. Revisiting label smoothing and knowledge distillation compatibility: What was missing? In *Proceedings of the 39th International Conference on Machine Learning*, volume 162 of *Proceedings of Machine Learning Research*, pages 2890–2916. PMLR, 17-23 Jul 2022.
- [53] Jing Yu Koh, Ruslan Salakhutdinov, and Daniel Fried. Grounding language models to images for multi-modal generation. *arXiv preprint arXiv:2301.13823*, 2023.
- [54] Keshigeyan Chandrasegaran, Ngoc-Trung Tran, Alexander Binder, and Ngai-Man Cheung. Discovering transferable forensic features for cnn-generated images detection. In *Proceedings of the European Conference on Computer Vision (ECCV)*, Oct 2022.
- [55] Prannay Khosla, Piotr Teterwak, Chen Wang, Aaron Sarna, Yonglong Tian, Phillip Isola, Aaron Maschinot, Ce Liu, and Dilip Krishnan. Supervised contrastive learning. *Advances in neural information processing systems*, 33:18661–18673, 2020.

Supplementary Materials

In this supplementary material, we provide additional experiments, analysis, ablation study, and details required to reproduce our results. Pytorch code, demo, pre-trained models and reconstructed data are available at our [project website](#).

Contents

A	Additional Analysis and Visualizations	16
A.1	Our Surrogate models are effective proxies for the opaque Target model for MI . . .	16
A.2	Decision knowledge transfer to T-ACGAN during training	17
B	Additional results	22
B.1	Different white-box attacks with surrogate models	22
B.2	Different TACGAN architecture	22
B.3	White-box attack results for reference	22
B.4	Model stealing	23
B.5	Architecture selection for Surrogate models	23
C	Additional Reconstruction Results	24
D	Experiment details/ Design choices	25
E	Evaluation details	26
E.1	T-ACGAN architecture	26
E.2	Hyperparameters	26
E.3	User study	27
F	Related works	27
G	Additional information for checklist	29

A Additional Analysis and Visualizations

A.1 Our Surrogate models are effective proxies for the opaque Target model for MI

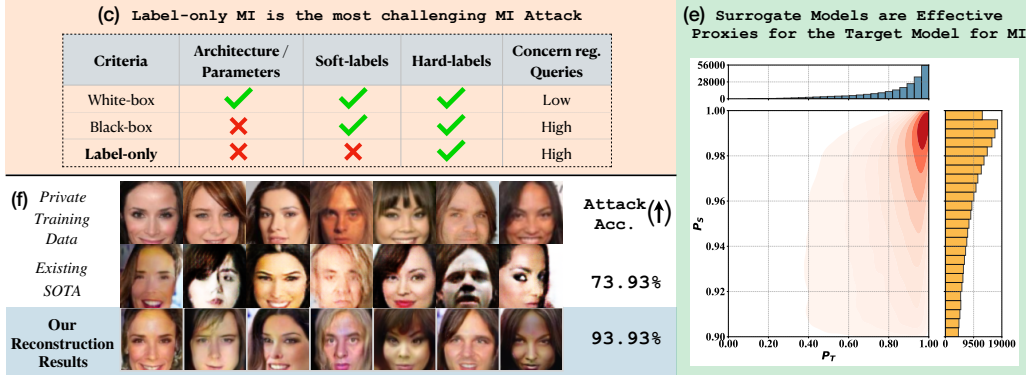


Figure A.1: We use $\mathcal{D}_{priv} = \text{CelebA}$, $\mathcal{D}_{pub} = \text{CelebA}$, $T = \text{FaceNet64}$, $S = \text{DenseNet-161}$. (c) We cast the challenging problem setup of label-only MI attack as a white-box MI attack. To our knowledge, our proposed approach is the first to address label-only MI via white-box MI attacks. (e) We consider high likelihood samples under S , i.e.: $P_S > 0.9$. Our analysis using 500k training data demonstrates that S is an effective proxy for T for MI attack. In particular, the white-box MI attack on S mimics the white-box attack on opaque T . (f) Additional reconstruction results using our proposed approach (S_{en}). We remark that our proposed approach significantly improves the Label-only MI attack (e.g. $\approx 20\%$ improvement in standard CelebA benchmark compared to existing SOTA [6]) resulting in significant improvement in private data reconstruction. Best viewed in color.

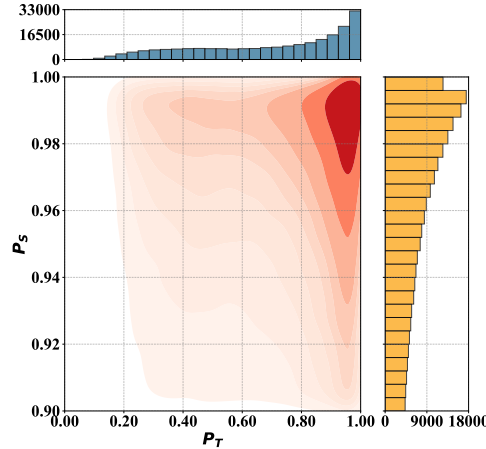


Figure A.2: Figure 1 (e) from the main paper supports that S is a good proxy for T for MI established using **Property P1**. We use $\mathcal{D}_{priv} = \text{CelebA}$, $\mathcal{D}_{pub} = \text{CelebA}$, $T = \text{FaceNet64}$, $S = \text{DenseNet-161}$. We use 500k validation data for analysis.

White-box MI attack on S mimics the white-box attack on T . For clarity, we copy **Figure 1(e)** (main paper) to Supplementary Fig. A.2. In this section, we include the details of Fig. A.2 and provide additional empirical evidence in Figure A.1(e) to support **Property P1**. We remark that Fig. A.2 and Fig. A.1(e) use 500k validation and 500k training data respectively[‡]. In both figures, we consider high-likelihood samples under S , i.e.: $P_S > 0.90$. We remark that since in our framework, we optimize white-box attack w.r.t. S , the reconstructed samples usually have a very high likelihood under S (above 0.9). Therefore, we condition our analysis on $P_S > 0.9$. As one can clearly observe in both conditional P_T histograms in Fig. A.2 and Fig. A.1(e), high likelihood samples under S are

[‡]We recall that the data samples are generated samples from our T-ACGAN. Using generated samples for analysis is suitable as generated samples are utilized during white-box MI.

likely to have high likelihood under T (**Property P1**), and it is uncommon for high likelihood samples under S to have low likelihood under T . Given **P1**, white-box attacks on S can mimic white-box attacks on T , resulting in S being an effective proxy for T for MI. In addition, we report similar observations on another setup: \mathcal{D}_{priv} =CelebA, \mathcal{D}_{pub} =FFHQ, T =FaceNet64, S =DenseNet-161 in Fig. A.3.

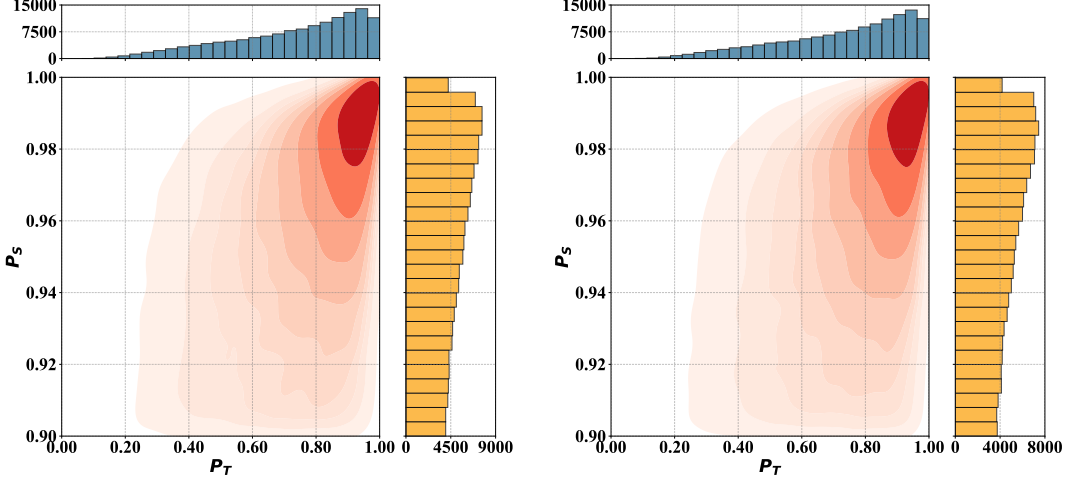


Figure A.3: We use \mathcal{D}_{priv} = CelebA, \mathcal{D}_{pub} = FFHQ, T = FaceNet64, S = DenseNet-161. we consider high likelihood samples under S . i.e.: $P_S > 0.90$, and show results for 500k training samples (left) and 500k validation samples (right). As one can clearly observe in both conditional P_T histograms, high likelihood samples under S are likely to have high likelihood under T (**Property P1**), and it is uncommon for high likelihood samples under S to have low likelihood under T . Given **P1**, white-box attacks on S can mimic white-box attacks on T , resulting in S being an effective proxy of T for MI.

Why would S possess **P1?** We provide additional empirical results using training and validation sets to support why S possesses **P1** using the framework by [35]. We use publicly available SOTA face recognition model(s) ** to extract face embeddings (128-dimensional) for analysis. We use the following setup for analysis: \mathcal{D}_{priv} = CelebA [40], \mathcal{D}_{pub} = CelebA [40], T = FaceNet64, S = DenseNet-161. Based on the distance from the face-embedding centroid for each identity, we consider the closest 70% of samples as easy samples, and the remaining 30% samples as hard samples ††. The training dynamic results for easy and hard samples for 3 sets of randomly chosen identities are shown in Fig. A.4, A.5 and A.6, for both training and validation sets. We also show the training dynamics for the validation set corresponding to the main paper analysis results in Fig. A.7.

A.2 Decision knowledge transfer to T-ACGAN during training

In this section, we provide additional analysis to support that the target model, T 's, decision knowledge is adequately transferred to our T-ACGAN during training. Following the definition in Sec. 4.3 (main paper), $x_f = G(z, y)$, $\tilde{y} = T(x_f)$, let γ be the percentage of samples with y the same as \tilde{y} in a batch of samples. In particular, we track γ throughout our T-ACGAN training. Initially, we expect γ to be low and with increasing training iterations, we expect γ to increase indicating adequate decision knowledge transfer from the target model T . We report γ tracking results for 2 experiment setups in Fig. A.8. • **Setup 1:** We use \mathcal{D}_{priv} = CelebA [40], \mathcal{D}_{pub} = CelebA [40], T = FaceNet64. • **Setup 2:** We use \mathcal{D}_{priv} = CelebA [40], \mathcal{D}_{pub} = FFHQ [43], T = FaceNet64. We remark that batch size=128 as we track γ for every batch. We train T-ACGAN for 100k iterations. As one can observe, γ starts low and gradually increases during T-ACGAN training indicating adequate knowledge transfer from T .

**https://github.com/ageitgey/face_recognition

††Note that the 70:30 selection of easy:hard samples has no effect to our algorithm; in fact our algorithm does not need explicit separation of easy/hard samples. Here in this discussion, we separate easy and hard samples only to ease our illustration of *different pace of P_S improvement among the samples*, which results in most samples with $P_S > 0.9$ having high P_T .

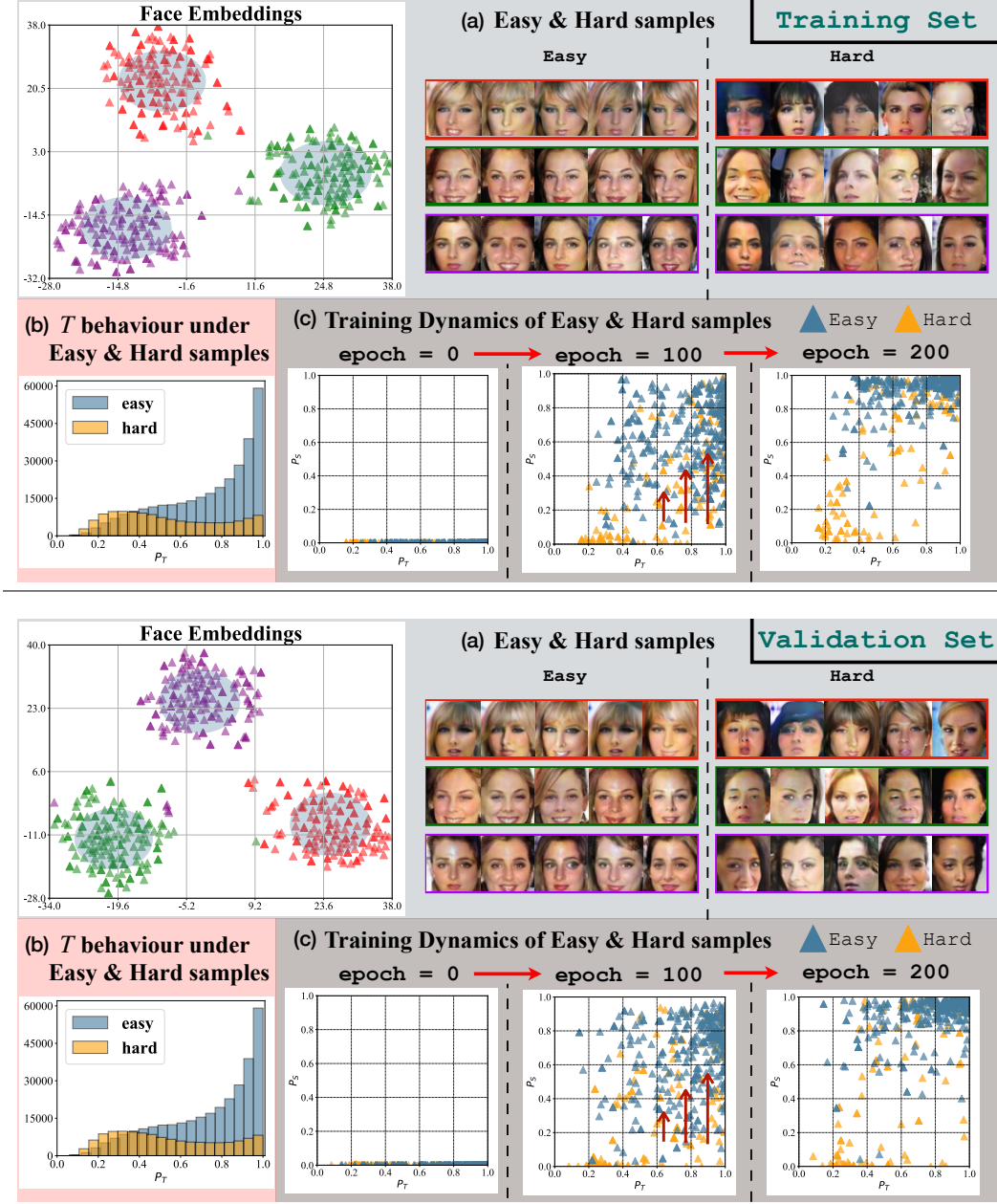


Figure A.4: We use $\mathcal{D}_{priv} = \text{CelebA}$ [40], $\mathcal{D}_{pub} = \text{CelebA}$ [40], $T = \text{FaceNet64}$, $S = \text{DenseNet-161}$. The face embeddings are extracted using publicly available SOTA face recognition models here. Similar to our main paper, we apply the framework of [35] to analyze learning dynamics of S to reason why S possesses **P1**, and therefore could be an effective proxy for T under MI. We analyze generated samples x_f from our T-ACGAN for 3 identities (IDs 49, 34, 58). We use 150 samples for each identity, and show results for both training set (top) and validation set (bottom). Note that x_f analysis is relevant as generated samples are used in MI attacks. (a): Different clusters and different distances from cluster centroids can be observed, suggesting patterns of face identities in some samples (easy samples) while diverse appearance in other samples (hard samples). We use distances from centroids to identify easy samples x_f^e and hard samples x_f^h (easy samples are indicated using a transparent blue circle for each ID in the visualization). Visualization of x_f^e and x_f^h in image space further demonstrates identity patterns in x_f^e and diverse appearance in x_f^h . (b): Similar to [35], we observe that x_f^e and x_f^h tend to have high and low likelihood under T (P_T) resp. This is shown using 500k training data (top) and 500k validation data (bottom). (c): We track likelihood under S (P_S) for x_f^e and x_f^h during the training of S . As training progresses, P_S of x_f^e and x_f^h improve in general, and samples move up vertically (note that P_T of samples do not change). Consistent with the “DNNs Learn Patterns First” finding in [35], S learns general identity patterns first to fit the easy samples. Therefore, P_S of x_f^e improve at a faster pace in the training, and many of them achieve high P_S at epoch = 200. As x_f^e tend to have high P_T , we observe property **P1** in S . For x_f^h (many of them tend to have low P_T), it is uncommon for S to achieve high likelihood on them as they do not fit easily to the pattern learned by S . Best viewed in color.

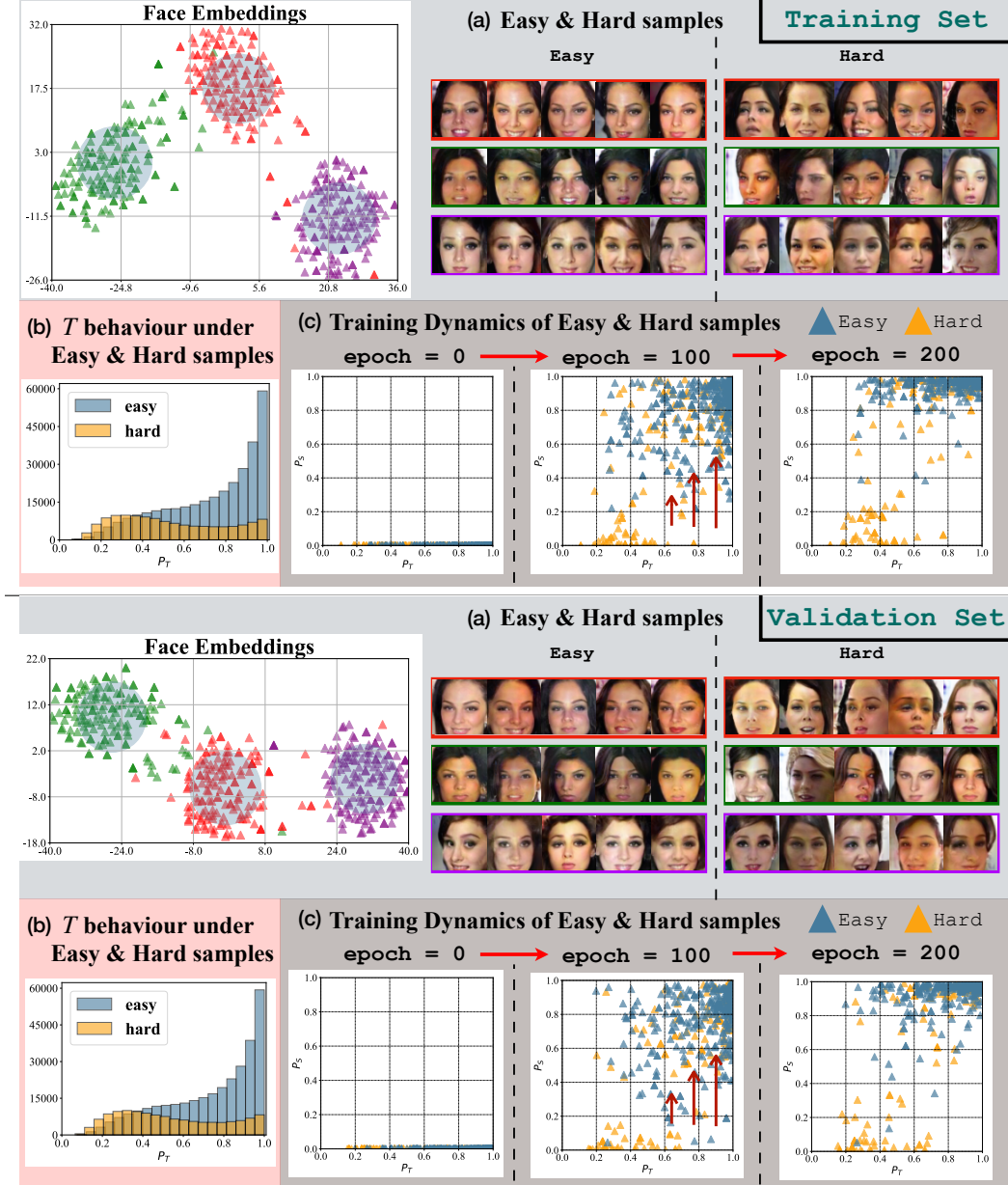


Figure A.5: We use $\mathcal{D}_{priv} = \text{CelebA}$ [40], $\mathcal{D}_{pub} = \text{CelebA}$ [40], $T = \text{FaceNet64}$, $S = \text{DenseNet-161}$. The face embeddings are extracted using publicly available SOTA face recognition models here. Similar to our main paper, we apply the framework of [35] to analyze learning dynamics of S to reason why S possesses **P1**, and therefore could be an effective proxy for T under MI. We analyze generated samples x_f from our T-ACGAN for 3 identities (IDs 71, 64, 93). We use 150 samples for each identity and show results for both the training set (top) and the validation set (bottom). Note that x_f analysis is relevant as generated samples are used in MI attacks. (a): Different clusters and different distances from cluster centroids can be observed, suggesting patterns of face identities in some samples (easy samples) while diverse appearance in other samples (hard samples). We use distances from centroids to identify easy samples x_f^e and hard samples x_f^h (easy samples are indicated using a transparent blue circle for each ID in the visualization). Visualization of x_f^e and x_f^h in image space further demonstrates identity patterns in x_f^e and diverse appearance in x_f^h . (b): Similar to [35], we observe that x_f^e and x_f^h tend to have high and low likelihood under T (P_T) resp. This is shown using 500k training data (top) and 500k validation data (bottom). (c): We track likelihood under S (P_S) for x_f^e and x_f^h during the training of S . As training progresses, P_S of x_f^e and x_f^h improve in general, and samples move up vertically (note that P_T of samples do not change). Consistent with the “DNNs Learn Patterns First” finding in [35], S learns general identity patterns first to fit the easy samples. Therefore, P_S of x_f^e improve at a faster pace in the training, and many of them achieve high P_S at epoch = 200. As x_f^e tend to have high P_T , we observe property **P1** in S . For x_f^h (many of them tend to have low P_T), it is uncommon for S to achieve high likelihood on them as they do not fit easily to the pattern learned by S . Best viewed in color.



Figure A.6: We use $\mathcal{D}_{priv} = \text{CelebA}$ [40], $\mathcal{D}_{pub} = \text{CelebA}$ [40], $T = \text{FaceNet64}$, $S = \text{DenseNet-161}$. The face embeddings are extracted using publicly available SOTA face recognition models here. Similar to our main paper, we apply the framework of [35] to analyze learning dynamics of S to reason why S possesses **P1**, and therefore could be an effective proxy for T under MI. We analyze generated samples x_f from our T-ACGAN for 3 identities (IDs 121, 95, 163). We use 150 samples for each identity and show results for both the training set (top) and the validation set (bottom). Note that x_f analysis is relevant as generated samples are used in MI attacks. **(a):** Different clusters and different distances from cluster centroids can be observed, suggesting patterns of face identities in some samples (easy samples) while diverse appearance in other samples (hard samples). We use distances from centroids to identify easy samples x_f^e and hard samples x_f^h (easy samples are indicated using a transparent blue circle for each ID in the visualization). Visualization of x_f^e and x_f^h in image space further demonstrates identity patterns in x_f^e and diverse appearance in x_f^h . **(b):** Similar to [35], we observe that x_f^e and x_f^h tend to have high and low likelihood under T (P_T) resp. This is shown using 500k training data (top) and 500k validation data (bottom). **(c):** We track likelihood under S (P_S) for x_f^e and x_f^h during the training of S . As training progresses, P_S of x_f^e and x_f^h improve in general, and samples move up vertically (note that P_T of samples do not change). Consistent with the “DNNs Learn Patterns First” finding in [35], S learns general identity patterns first to fit the easy samples. Therefore, P_S of x_f^e improve at a faster pace in the training, and many of them achieve high P_S at epoch = 200. As x_f^e tend to have high P_T , we observe property **P1** in S . For x_f^h (many of them tend to have low P_T), it is uncommon for S to achieve high likelihood on them as they do not fit easily to the pattern learned by S . Best viewed in color.

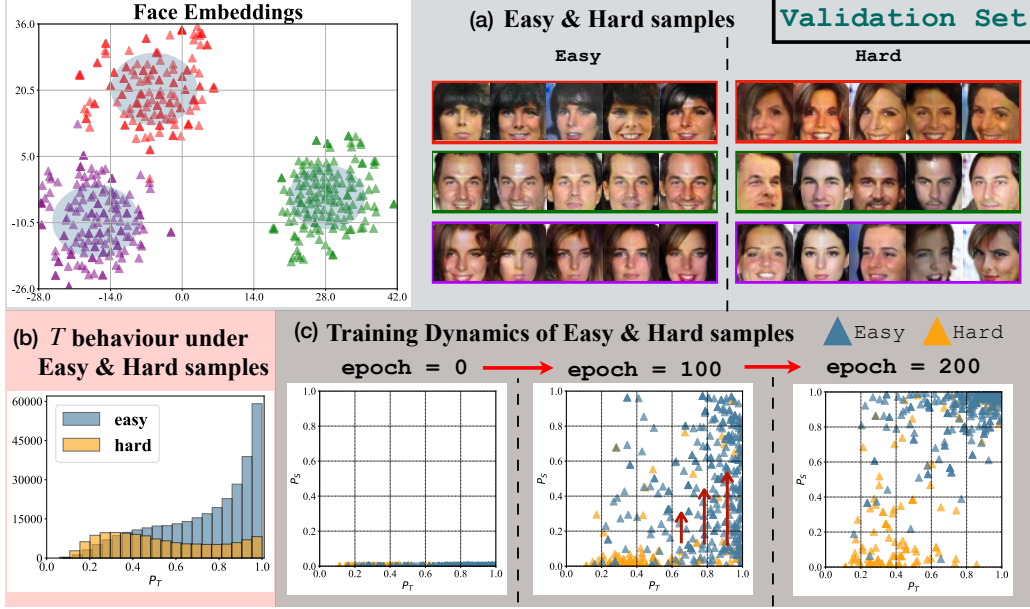


Figure A.7: We use $\mathcal{D}_{priv} = \text{CelebA}$ [40], $\mathcal{D}_{pub} = \text{CelebA}$ [40], $T = \text{FaceNet64}$, $S = \text{DenseNet-161}$. The face embeddings are extracted using publicly available SOTA face recognition models here. Similar to our main paper, we apply the framework of [35] to analyze learning dynamics of S to reason why S possesses **P1**, and therefore could be an effective proxy for T under MI. We analyze generated samples x_f from our T-ACGAN for 3 identities (IDs 20, 16, 36). We use 150 samples for each identity and show results for the validation set. The training set results are already shown in the [main paper Fig. 2](#). Note that x_f analysis is relevant as generated samples are used in MI attacks. (a): Different clusters and different distances from cluster centroids can be observed, suggesting patterns of face identities in some samples (easy samples) while diverse appearance in other samples (hard samples). We use distances from centroids to identify easy samples x_f^e and hard samples x_f^h (easy samples are indicated using a transparent blue circle for each ID in the visualization). Visualization of x_f^e and x_f^h in image space further demonstrates identity patterns in x_f^e and diverse appearance in x_f^h . (b): Similar to [35], we observe that x_f^e and x_f^h tend to have high and low likelihood under T (P_T) resp. This is shown using 500k training data (top) and 500k validation data. (c): We track likelihood under S (P_S) for x_f^e and x_f^h during the training of S . As training progresses, P_S of x_f^e and x_f^h improve in general, and samples move up vertically (note that P_T of samples do not change). Consistent with the “DNNs Learn Patterns First” finding in [35], S learns general identity patterns first to fit the easy samples. Therefore, P_S of x_f^e improve at a faster pace in the training, and many of them achieve high P_S at epoch = 200. As x_f^e tend to have high P_T , we observe property **P1** in S . For x_f^h (many of them tend to have low P_T), it is uncommon for S to achieve high likelihood on them as they do not fit easily to the pattern learned by S . Best viewed in color.

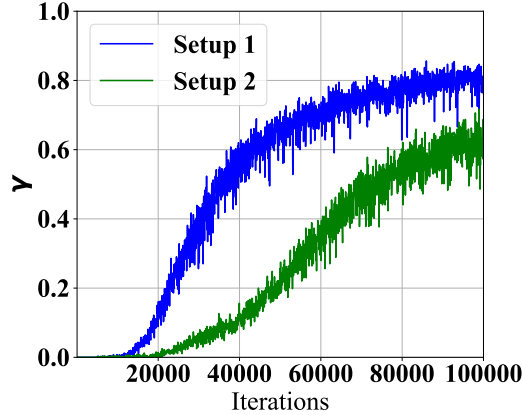


Figure A.8: We report γ tracking results during T-ACGAN training for 2 setups. Our T-ACGAN is trained for 100k iterations. In both setups, γ starts low ($\gamma \approx 0$ for iterations less than 5000). With increasing iterations, γ increases indicating adequate decision knowledge transfer from the target model T to T-ACGAN. We remark that **Setup 2** has lower γ in general compared to **Setup 1** due to a large distribution shift between public data and private data.

B Additional results

B.1 Different white-box attacks with surrogate models

In this section, we perform a set of experiments to demonstrate that the surrogate models trained using our proposed framework are versatile enough to be used with different white-box MI attacks. For this analysis, we use two SOTA white-box attacks, namely KEDMI [2] and PLGMI [7]. For each white-box attack, we train five different surrogate models using our proposed framework including: $C \circ D$, S_{DN121} = Desenet-121, S_{DN161} = Desenet-161, S_{DN169} = Desenet-169, and $S_{en} = \{\text{Desenet-121, Desenet-161, Desenet-169}\}$, and then, evaluate the white-box MI attack performance on each of these surrogate models.

In the case of KEDMI, we train a specific-GAN using our surrogate model S using the official implementation^{‡‡}. As for PLGMI^{§§}, given that our T-ACGAN can serve as a replacement for the conditional GAN of PLGMI, we leverage our T-ACGAN to apply the PLGMI attack. It is noteworthy that the target classifier T is not used during the attacks when we apply white-box attacks on our surrogate models.

We report the results in Table B.1, utilizing the CelebA dataset setup. Our results demonstrate the effectiveness of our surrogate models using white-box MI attacks, and are consistent with the outcomes obtained using the target classifier T in white-box attacks.

Table B.1: We compare the attack results using different white-box attacks with five surrogate models. We use T = FaceNet64, \mathcal{D}_{priv} = CelebA, \mathcal{D}_{pub} = CelebA. The results show that our different designs of surrogate model perform well across different white-box attacks. Note that the white-box attack results on T are included only as reference as our setup does not have access to T parameters nor soft-label of T .

Attack	Model	Attack acc. \uparrow	KNN dt. \downarrow
KEDMI	T [2]	81.13 ± 4.66	1298.63
	$C \circ D$	42.07 ± 3.46	1473.99
	S_{DN121}	62.93 ± 4.67	1350.67
	S_{DN161}	65.07 ± 3.79	1351.07
	S_{DN169}	62.80 ± 4.45	1350.56
	S_{en}	69.00 ± 4.03	1329.84
	T [7]	99.00 ± 0.01	1103.03
PLGMI	$C \circ D$	81.00 ± 4.79	1298.63
	S_{DN121}	92.27 ± 2.85	1208.55
	S_{DN161}	92.80 ± 2.59	1207.25
	S_{DN169}	92.33 ± 3.36	1206.15
	S_{en}	93.93 ± 2.78	1181.72

B.2 Different TACGAN architecture

For a fair comparison with BREPMI [6], we provide the experiment results by training a new T-ACGAN using the same architectures as the GAN used by BREPMI. For the discriminator (D), we apply max pooling and add a linear layer before the last layer for the classifier head. As for the generator (G), we retain the same architecture and replace batch normalization with conditional batch normalization.

We report the results in Table B.2. Our results are better than BREPMI when using the same GAN architecture.

B.3 White-box attack results for reference

We show the our proposed method and other SOTA white-box attacks including GMI [1], KEDMI [2], PLGMI [7], and the SOTA label-only attack BREPMI [6] in Table B.3 for reference.

^{‡‡}<https://github.com/SCccc21/Knowledge-Enriched-DMI>

^{§§}<https://github.com/LetheSec/PLG-MI-Attack>

Table B.2: We conduct comprehensive comparison between our proposed method and existing SOTA BREPMI [6] using the same GAN architecture. Specifically, we evaluate the performance of our three proposed designs of surrogate, namely $C \circ D$, S , and S_{en} , while BREPMI performs black-box search on T directly. We highlight the best results in each setup in **bold**.

Setup	Attack	Attack acc. \uparrow	KNN dt. \downarrow
T = FaceNet64	BREPMI	73.93 ± 4.98	1284.41
\mathcal{D}_{priv} = CelebA	$C \circ D$	85.47 ± 2.95	1336.45
\mathcal{D}_{pub} = CelebA	LOKT S	90.73 ± 3.57	1251.16
	S_{en}	93.20 ± 1.98	1214.60
T = IR152	BREPMI	71.47 ± 5.32	1277.23
\mathcal{D}_{priv} = CelebA	$C \circ D$	88.20 ± 3.48	1304.05
\mathcal{D}_{pub} = CelebA	LOKT S	92.27 ± 2.46	1236.87
	S_{en}	94.53 ± 2.34	1214.38
T = VGG16	BREPMI	57.40 ± 4.92	1376.94
\mathcal{D}_{priv} = CelebA	$C \circ D$	68.93 ± 4.23	1450.74
\mathcal{D}_{pub} = CelebA	LOKT S	78.07 ± 2.91	1362.70
	S_{en}	82.80 ± 3.20	1346.51
T = FaceNet64	BREPMI	43.00 ± 5.14	1470.55
\mathcal{D}_{priv} = CelebA	$C \circ D$	59.87 ± 5.05	1509.09
\mathcal{D}_{pub} = FFHQ	LOKT S	67.20 ± 4.23	1467.62
	S_{en}	72.33 ± 3.30	1454.43

B.4 Model stealing

One related area to training surrogate models for a target model is *model stealing* where an attacker aims to copy the performance of a target model. In this section, we compare the performance of our proposed method for training surrogate models—specifically designed for MI attacks—with model stealing approaches. More specifically, we apply the SOTA model stealing approach DFMS-HL ^{¶¶} [46] that only uses the hard labels to train the surrogate model S . We train two surrogate models $S = C \circ D$, and $S = \text{Densenet-161}$ [45] using DFMS-HL and compare it with the trained surrogate models with the proposed approach. Table B.4 shows that the surrogate models trained with our proposed method can perform much better for MI attacks.

B.5 Architecture selection for Surrogate models

Our proposed approach (casting label-only MI attack as white-box MI attack) allows the possibility for MI attackers to choose the surrogate model architecture(s). In this section, we study the effect of model architectures on model accuracy and MI attack accuracy to empirically justify our use of DenseNet model variants [45] as surrogate models. The details of this study is as follows: We conduct MI attacks on three different model families including MobileNet (MobileNetV2 [47] and MobileNetV3-small/large [48]), EfficientNet [49] (EfficientNet-B0, EfficientNet-B1, EfficientNet-B2, EfficientNet-B3, EfficientNet-B4, EfficientNet-B7), and DenseNet [45] (DenseNet-121, DenseNet-161, DenseNet-169). The number of parameters for each model (in Millions) is given in Table B.5. We first train these 12 model architectures using private dataset $\mathcal{D}_{priv} = \text{CelebA}$ [40] which contains 30,027 images/1,000 identities following the exact training protocol in [2].

After training target models, we perform white-box MI attacks on these target models. We use two popular white-box MI attacks namely GMI [1] and KEDMI [2]. Following [2], we use evaluation model $E = \text{FaceNet}$ [36]. We report the model accuracy and MI attack accuracy in Fig. B.1. When comparing models within the same family, in general, we observe that architectures with more parameters achieve better model accuracy and are more susceptible to MI attacks (Higher MI Attack Acc). Based on KEDMI [2] results obtained in this study, *we use architectures from the DenseNet family*^{***}.

^{¶¶}<https://github.com/val-iisc/Hard-Label-Model-Stealing>

^{***}DenseNet-161 has more parameters than DenseNet-169 More details: as our surrogate model(s)

Table B.3: We evaluate the performance of our label-only attack method across various experimental setups. For reference, we also include our results against three state-of-the-art (SOTA) white-box attacks, namely GMI [1], KEDMI [2], PLGMI [7], as well as the SOTA label-only attack BREPMI [6]. The obtained results clearly demonstrate the effectiveness of our label-only attack method over BREPMI, while also achieving comparable performance with other white-box attacks.

Label-only MI Attacks			White-box MI Attacks (for reference only)							
	LOKT		BREPMI [6]		GMI [1]		KEDMI [2]		PLGMI [7]	
S	Attack acc. \uparrow	KNN dt. \downarrow	Attack acc. \uparrow	KNN dt. \downarrow	Attack acc. \uparrow	KNN dt. \downarrow	Attack acc. \uparrow	KNN dt. \downarrow	Attack acc. \uparrow	KNN dt. \downarrow
$T = \text{FaceNet64}, \mathcal{D}_{\text{priv}} = \text{CelebA}, \mathcal{D}_{\text{pub}} = \text{CelebA}$										
$C \circ D$	81.00 \pm 4.79	1298.63	73.93 \pm 4.98	1284.41	26.20 \pm 4.66	1626.60	81.13 \pm 4.66	1247.91	99.00 \pm 0.01	1103.03
S	92.80 \pm 2.59	1207.25								
S_{en}	93.93 \pm 2.78	1181.72								
$T = \text{IR152}, \mathcal{D}_{\text{priv}} = \text{CelebA}, \mathcal{D}_{\text{pub}} = \text{CelebA}$										
$C \circ D$	72.07 \pm 4.03	1358.94	71.47 \pm 5.32	1277.23	29.47 \pm 4.70	1609.57	79.87 \pm 3.52	1251.37	100.0 \pm 0.00	1026.71
S	89.80 \pm 2.33	1220.00								
S_{en}	92.13 \pm 2.06	1206.78								
$T = \text{VGG16}, \mathcal{D}_{\text{priv}} = \text{CelebA}, \mathcal{D}_{\text{pub}} = \text{CelebA}$										
$C \circ D$	71.33 \pm 4.39	1364.47	57.40 \pm 4.92	1376.94	18.07 \pm 4.44	1705.04	74.07 \pm 4.21	1290.81	97.00 \pm 0.01	1120.61
S	85.60 \pm 3.03	1252.09								
S_{en}	87.27 \pm 1.97	1246.71								
$T = \text{BiDO-HSIC [39]}, \mathcal{D}_{\text{priv}} = \text{CelebA}, \mathcal{D}_{\text{pub}} = \text{CelebA}$										
$C \circ D$	45.73 \pm 5.94	1493.48	37.40 \pm 3.66	1500.45	5.93 \pm 1.85	1930.52	42.80 \pm 4.58	1478.32	87.53 \pm 3.08	1237.41
S	58.53 \pm 4.87	1427.22								
S_{en}	60.73 \pm 3.07	1395.93								
$T = \text{FaceNet64}, \mathcal{D}_{\text{priv}} = \text{Facescrub}, \mathcal{D}_{\text{pub}} = \text{Facescrub}$										
$C \circ D$	45.70 \pm 4.00	1296.29	40.20 \pm 6.60	1236.40	14.60 \pm 3.70	1599.67	55.20 \pm 4.61	1193.41	92.50 \pm 2.91	1012.74
S	53.20 \pm 5.29	1280.70								
S_{en}	58.60 \pm 4.86	1225.13								
$T = \text{FaceNet64}, \mathcal{D}_{\text{priv}} = \text{Pubfig83}, \mathcal{D}_{\text{pub}} = \text{Pubfig83}$										
$C \circ D$	74.80 \pm 5.93	924.58	55.60 \pm 4.34	1012.83	16.40 \pm 4.77	1338.61	66.00 \pm 4.00	1031.86	99.60 \pm 0.89	832.07
S	61.60 \pm 3.58	995.08								
S_{en}	80.00 \pm 3.16	883.52								
$T = \text{FaceNet64}, \mathcal{D}_{\text{priv}} = \text{CelebA}, \mathcal{D}_{\text{pub}} = \text{FFHQ}$										
$C \circ D$	43.27 \pm 3.53	1516.18	43.00 \pm 5.14	1470.55	11.00 \pm 4.64	1750.74	54.20 \pm 5.16	1443.44	95.00 \pm 0.04	1241.41
S	59.13 \pm 2.77	1437.86								
S_{en}	62.07 \pm 3.89	1428.04								
$T = \text{FaceNet64}, \mathcal{D}_{\text{priv}} = \text{Facescrub}, \mathcal{D}_{\text{pub}} = \text{FFHQ}$										
$C \circ D$	44.50 \pm 5.98	1403.73	37.30 \pm 3.99	1456.59	11.00 \pm 3.63	1864.71	50.80 \pm 4.58	1337.96	89.10 \pm 3.05	1196.88
S	47.20 \pm 4.39	1404.85								
S_{en}	53.70 \pm 4.57	1338.67								
$T = \text{FaceNet64}, \mathcal{D}_{\text{priv}} = \text{Pubfig83}, \mathcal{D}_{\text{pub}} = \text{FFHQ}$										
$C \circ D$	85.60 \pm 2.61	914.15	72.80 \pm 3.90	971.51	36.40 \pm 5.55	1199.00	84.00 \pm 4.00	891.21	100.0 \pm 0.00	787.57
S	88.40 \pm 2.97	920.99								
S_{en}	94.40 \pm 3.85	862.24								

Table B.4: The comparison on MI attacks results using our surrogate models and model stealing DFMS-HL [46]. Here we use PLGMI [7], $\mathcal{D}_{\text{priv}} = \text{CelebA}$, $\mathcal{D}_{\text{pub}} = \text{CelebA}$, $T = \text{FaceNet64}$.

S	DFMS-HL [46]		LOKT	
	Attack Acc. \uparrow	KNN dt. \downarrow	Attack Acc. \uparrow	KNN dt. \downarrow
$C \circ D$	14.00 \pm 4.01	1775.71	81.00 \pm 4.79	1298.63
Densenet-161	67.13 \pm 3.67	1411.45	92.80 \pm 2.59	1207.25

Table B.5: Number of parameters (in Millions) for different model architectures.

Model	Mobi_small	Mobi_large	Mobi_v2	Eff-B0	Eff-B1	Eff-B2	Eff-B3	Eff-B4	Eff-B7	Den-121	Den-161	Den-169
Parameters (M)	1.50	3.93	3.50	5.29	7.79	9.11	12.20	19.30	66.30	11.10	35.30	19.10

C Additional Reconstruction Results

In this section, we show reconstructed samples for 3 additional setups using our proposed method. We show cross-dataset MI results in Fig. C.2 using FaceNet64 target model. In addition, we also

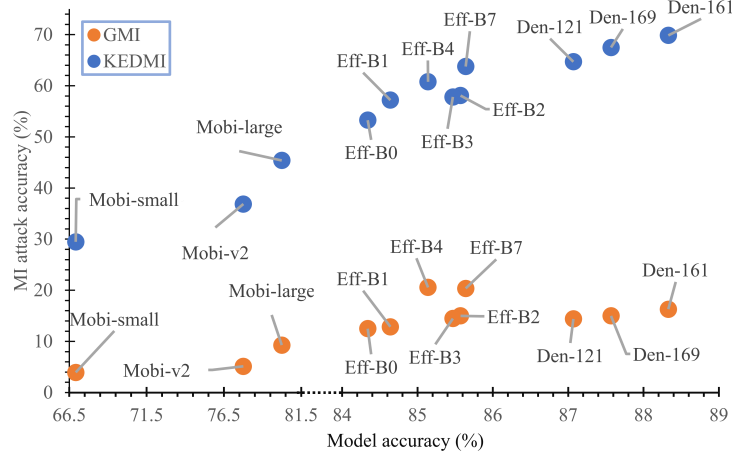


Figure B.1: *Architecture selection for surrogate models*: We report model accuracy and MI attack accuracy of 12 models from 3 model families namely, MobileNet (MobileNetV2 [47] and MobileNetV3-small/ large [48]), EfficientNet [49] (EfficientNet-B0, EfficientNet-B1, EfficientNet-B2, EfficientNet-B3, EfficientNet-B4, EfficientNet-B7), and DenseNet [45] (DenseNet-121, DenseNet-161, DenseNet-169). The number of parameters for each model is included in Table B.5. • We observe that compact models such as MobileNets obtain relatively lower model accuracy and lower MI Attack accuracy. • We observe that larger models, i.e.: DenseNet models, achieve relatively higher model accuracy and higher MI Attack accuracy making them good candidates for surrogate models.

show results for 2 additional target models: IR152 [37] and VGG16 [38] in Fig. C.3 and Fig. C.4 respectively.



Figure C.2: We use $\mathcal{D}_{priv} = \text{CelebA}$ [40], $\mathcal{D}_{pub} = \text{FFHQ}$ [43], $T = \text{FaceNet64}$. We show private data (top), *our* reconstruction results (bottom) and Attack accuracy. We remark that these results are obtained using S_{en} .



Figure C.3: We use $\mathcal{D}_{priv} = \text{CelebA}$ [40], $\mathcal{D}_{pub} = \text{CelebA}$ [40], $T = \text{IR152}$ [37]. We show private data (top), *our* reconstruction results (bottom) and Attack accuracy. We remark that these results are obtained using S_{en} .

D Experiment details/ Design choices

We use three datasets including CelebA [40], Facescrub [41], and Pubfig83 [42]. We further examine the distribution shift by using FFHQ dataset [43] which includes images that vary in terms of background, ethnicity, and age. Following [2, 6], we divide CelebA into two datasets \mathcal{D}_{priv} for training the target model T and \mathcal{D}_{pub} for training GAN and surrogate models \mathcal{C} . The details of each dataset are summarized in Table D.6.



Figure C.4: We use $\mathcal{D}_{priv} = \text{CelebA}$ [40], $\mathcal{D}_{pub} = \text{CelebA}$ [40], $T = \text{VGG16}$ [38]. We show private data (top), *our* reconstruction results (bottom) and Attack accuracy. We remark that these results are obtained using S_{en} .

Table D.6: Details of three datasets including CelebA [40], Facescrub [41], and Pubfig83 [42].

Dataset	\mathcal{D}_{priv}		\mathcal{D}_{pub}	
	# Target id	# Images	# Id	# Images
CelebA [40]	1,000	30,027	-	30,000
Facescrub [41]	200	40,953	330	65,910
Pubfig83 [42]	50	8,145	33	5,693
FFHQ [43]	-	-	-	70,000

E Evaluation details

Following [6], we attack the first 300 out of 1000 labels in the experiments using CelebA dataset. In cases of Facescrub and Pubfig, we attack all the labels of the target classifier (200 and 50, respectively). As for the evaluation model, we use FaceNet which is trained on the private dataset and has higher resolution than the target classifier (image resolution 112x112). We remark that all pre-trained target/evaluation models are released publicly by [6], and we adopt these models in our experiments for fair comparison.

E.1 T-ACGAN architecture

We adopt the SNResnet architecture [34, 44] for our T-ACGAN. The architecture of the generator and the discriminator are as shown in Table E.7 and E.8.

Table E.7: Generator

Operation	Kernel	Strides	Feature maps	BN?
Linear	N/A	N/A	16384	
Convolution	3x3	1x1	512	
Convolution	3x3	1x1	512	yes
Convolution	1x1	1x1	512	
Convolution	3x3	1x1	256	
Convolution	3x3	1x1	256	yes
Convolution	1x1	1x1	256	
Convolution	3x3	1x1	128	
Convolution	3x3	1x1	128	yes
Convolution	1x1	1x1	128	
Convolution	3x3	1x1	64	
Convolution	3x3	1x1	64	yes
Convolution	1x1	1x1	64	yes
Convolution	1x1	1x1	3	

E.2 Hyperparameters

Training T-ACGAN. The T-ACGAN model was trained using different numbers of iterations for CelebA [40], Facescrub [41], and Pubfig83 [42] datasets. Specifically, we utilized 20k iterations for CelebA, 5k iterations for Facescrub, and 3k iterations for Pubfig83. It's important to note that during training, the generator G was trained once while the discriminator D was trained five times for each iteration. For T-ACGAN loss, including generator loss \mathcal{L}_G , and discriminator loss $\mathcal{L}_{D,C}$

Table E.8: Discriminator. N is the number of classes.

Operation	Kernel	Strides	Feature maps
Convolution	3x3	1x1	64
Convolution	3x3	1x1	64
Convolution	1x1	1x1	64
Convolution	3x3	1x1	64
Convolution	3x3	1x1	128
Convolution	1x1	1x1	128
Convolution	3x3	1x1	128
Convolution	3x3	1x1	256
Convolution	1x1	1x1	256
Convolution	3x3	1x1	256
Convolution	3x3	1x1	512
Convolution	1x1	1x1	512
Convolution	3x3	1x1	512
Convolution	3x3	1x1	1024
Convolution	1x1	1	1024
Linear	N/A	N/A	1
Linear	N/A	N/A	N

(Eqn. (3) and (4) in the main paper), we select $\lambda_1 = 1.0$ and $\lambda_2 = 1.5$ for all experiments. This deliberate choice aims to enhance the learning process of both the generator and the discriminator by emphasizing the importance of conditional loss.

$$\mathcal{L}_G = \lambda_1 E[\log P(s = Fake|x_f)] - \lambda_2 E[\log P(c = y|x_f)]$$

$$\mathcal{L}_{D,C} = -\lambda_1 [E[\log P(s = Fake|x_f)] - E[\log P(s = Real|x_p)]] - \lambda_2 E[\log P(c = \tilde{y}|x_f)]$$

Training surrogate models S and S_{en} . As we mentioned in the main paper, to train additional surrogate models S and S_{en} , we create a new synthetic dataset generated by our T-ACGAN. Specially, we generate images using 500 pseudo labels for each class. These images are then labeled by the target classifier T . To train S and S_{en} , we use SGD optimizer with learning rate $lr = 0.1$, momentum 0.9 and weight decay 5×10^{-4} , and apply the CosineAnnealingLR scheduler [50].

Inversion. To reconstruct the images, after training the surrogate model S , in the main experimental results, we apply PLGMI [7] as the white-box MI attack on S using our T-ACGAN. For this reconstruction, we use Adam optimizer with the learning rate $lr = 0.002$ and optimize in 600 iterations as [7]. For other experiments, when using KEDMI and GMI as white-box MI attacks on S , following [2], we use SGD optimizer with learning rate $lr = 0.02$ and optimize in 2400 iterations.

E.3 User study

The user interface is shown in Figure E.5. The results are included in the main paper.

F Related works

Model Inversion (MI) aims to extract/ reconstruct the private information about the training data through a trained model. Depending on the level of information that can be accessed, MI attacks can be classified into three distinct categories: white-box attacks, black-box attacks, and label-only attacks.

White-Box MI Attack. In white-box attacks, the attacker is assumed to have complete access to the target model including model weights. Therefore, the MI attack is usually formulated as optimizing an identification loss:

$$x^* = \arg \min_x \mathcal{L}_{id}(x; y, T) \quad (5)$$

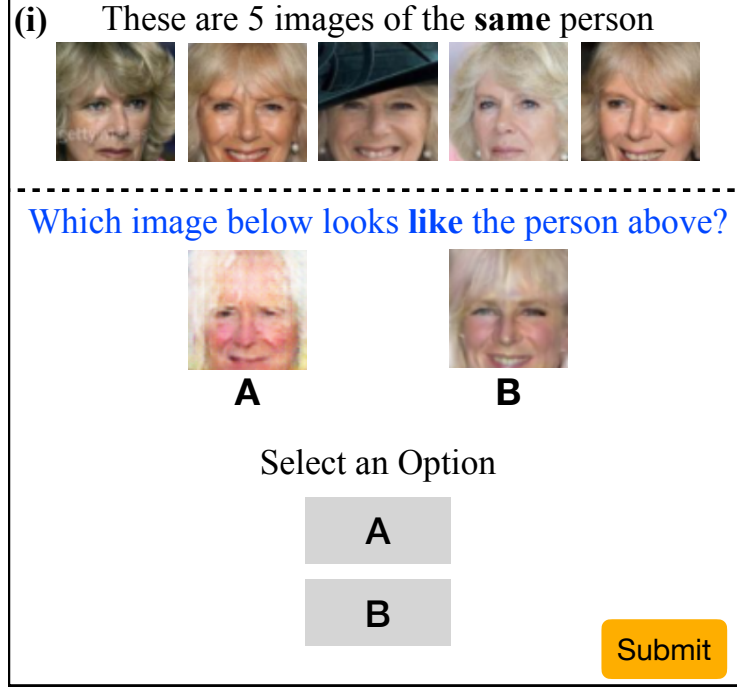


Figure E.5: **Human study setup/ user interface:** We follow the setup proposed by An *et al.* for human study. • In this setup, users are shown 5 real images of a person (identity) as reference. • Then users are required to compare the 5 real images with two inverted images: one from our method, the other from BREPMI. In the above example, A and B correspond to BREPMI and Ours respectively. The order is randomized for each task. Each user is given a maximum of 60 seconds per task, and each task is assigned to 10 unique users. Following [10], we randomly select 50 identities, resulting in 1000 pairs. We use Amazon Mechanical Turk service (MTurk). We use $D_{priv} = \text{CelebA}$, $D_{pub} = \text{CelebA}$, $T = \text{FaceNet64}$.

where $\mathcal{L}_{id}(x; y, T) = -\log \mathbb{P}_T(y|x)$, with $\mathbb{P}_T(y|x)$ denoting the probability (soft label) that the target model T classifies input x as label y . When handling a high-dimensional input data x like an image, performing the optimization (Eqn. 5) in input space ends up with degraded results [51, 1]. To overcome this issue, recent white-box approaches [1–3] constraint the search space into the manifold of related public images using a GAN. More specifically, GMI [1] proposes to train a GAN on a public dataset \mathcal{D}_{pub} , and perform the inversion step on the latent space of GAN:

$$z^* = \arg \min_z \mathcal{L}_{id}(z; y, T) + \lambda \mathcal{L}_{prior}(z) \quad (6)$$

where z^* denotes the optimal latent code which is later used by GAN to generate the reconstructed sample, i.e., $x^* = G(z^*)$. In addition, $\mathcal{L}_{prior} = -D(G(z))$ measures the realness of the generated sample. KEDMI [2] improves GMI by introducing inversion-specific GAN, and restoring a distribution of latent space instead of an optimal point. In addition, VMI [3] defines the variational inference in latent space. PLGMI [7] uses the target classifier to produce pseudo label for public data and trains a conditional GAN (cGAN) to limit the search space.

Black-Box MI Attack. In the black-box setup, the attackers have access to only model’s output and confidence scores (soft labels) which is very limited compared to the white-box setup. Due to this limitation, performing optimization discussed in Eqn. 5, and 6 become unfeasible in the black-box setup. Yang et al. [4] train an inversion model of the target model which serves as an encoder model specifically trained to produce the predicted score (soft labels). Simultaneously, the generator (decoder) is trained to generate the target image based on the predicted score of the inversion model.

Label-Only MI Attack. Label-only MI attack relies solely on the final decision of the model, i.e., the predicted label, without any additional information about the model or the confidence score of the prediction. Kahla et. al [6] propose Boundary-Repelling Model Inversion (BREP-MI) to address the model inversion attack under label-only setup. Beginning by initializing a random point that is

already classified into the target class, BREPMI evaluates the model’s predicted labels based on other neighbor points in the latent space and estimate the direction to reach the target class’s centroid.

In future work, we hope to explore different aspects of model inversion including multimodal learning, advanced knowledge transfer, data-centric applications and different types of generative models [17, 52–55, 21, 18].

G Additional information for checklist

Amount of Compute. The amount of compute in this project is reported in Table G.1. We follow NeurIPS guidelines to include the amount of compute for different experiments along with CO_2 emission.

Table G.1: Amount of compute in this project. The GPU hours include computations for initial explorations / experiments to produce the reported values. CO2 emission values are computed using <https://mlco2.github.io/impact/>

Experiment	Hardware	GPU hours	Carbon emitted in kg
Main paper : Table 3 (Repeated 3 times)	RTX A5000	306	29.56
Main paper : Table 2 and Table 4	RTX A5000	50	4.83
Main paper : Figure 1 / Figure 2	RTX A5000	4	0.39
Supplementary : All additional analysis/ Ablation study	RTX A5000	10	0.97
Additional Compute for Hyper-parameter tuning	RTX A5000	24	2.32
Total		394	38.07

Standard deviation of our experiments (Error Bars). We report the standard deviation of MI Attack accuracies for 2 experiment setups: • We use $\mathcal{D}_{priv} = \text{CelebA}$ [40], $\mathcal{D}_{pub} = \text{CelebA}$ [40], $T = \text{FaceNet64}$. • We use $\mathcal{D}_{priv} = \text{CelebA}$ [40], $\mathcal{D}_{pub} = \text{FFHQ}$ [43], $T = \text{FaceNet64}$. We repeated the entire training and experiments three times. For each trial, we trained T-ACGAN and surrogate models from scratch using different random seeds. The results are shown in Table G.2.

Table G.2: We report standard deviations for MI Attack accuracies for 2 experiment setups over 3 independent runs. The setups include: • We use $\mathcal{D}_{priv} = \text{CelebA}$ [40], $\mathcal{D}_{pub} = \text{CelebA}$ [40], $T = \text{FaceNet64}$. • We use $\mathcal{D}_{priv} = \text{CelebA}$ [40], $\mathcal{D}_{pub} = \text{FFHQ}$ [43], $T = \text{FaceNet64}$. We also report the standard deviations for existing SOTA [6].

Setup	Attack	Attack acc. \uparrow	KNN dt. \downarrow
$T = \text{FaceNet64}$	BREPMI	74.87 ± 4.17	1286.04 ± 1.42
$\mathcal{D}_{priv} = \text{CelebA}$	LOKT	$C \circ D$	80.80 ± 4.35
$\mathcal{D}_{pub} = \text{CelebA}$		S	1211.15 ± 17.06
		S_{en}	1193.16 ± 25.99
$T = \text{FaceNet64}$	BREPMI	41.91 ± 5.09	1484.20 ± 13.21
$\mathcal{D}_{priv} = \text{CelebA}$	LOKT	$C \circ D$	44.33 ± 4.25
$\mathcal{D}_{pub} = \text{FFHQ}$		S	1439.02 ± 13.79
		S_{en}	1426.89 ± 12.73